Hydraulics Research
Wallingford

THE NEARSHORE PROFILE MODEL

A computational model of wave and
current interaction in nearshore regions

H N Southgate MA

Report No SR 157
February 1988

Registered Office: Hydraulics Research Limited,
Wallingford, Oxfordshire OX10 8BA.
Telephone: 0491 35381. Telex: 848552

This report describes work carried out by Hydraulics Research into the movement of sand by combined waves and currents. It has been funded by the Ministry of Agriculture, Fisheries and Food under contract number CSA 992, the nominated officer being Mr A J Allison. At the time of reporting the Hydraulics Research nominated project officer was Dr S W Huntington.

The report is published on behalf of the Ministry of Agriculture, Fisheries and Food, but any opinions expressed within it are those of the author only, and are not necessarily those of the ministry who sponsored the research.

ABSTRACT

A computational model, known as the Nearshore Profile Model, has been developed at Hydraulics Research Ltd for predicting wave and current conditions in nearshore regions. This report describes the theory and computational techniques used by the model, and compares its predictions against laboratory and field data. The model uses the approximation of a straight coastline with parallel depth contours, and determines wave and current conditions at grid points along a shore-normal line. The theory of wave and current motion is based on general mass, energy and momentum balance equations which are applicable both inside and outside the surf zone, and includes some new approaches to the solutions of these equations. An important feature is the modelling of tidal currents as well as wave-induced currents, with full interaction between the two types of current and the waves. Because the model considers one horizontal dimension only, the computational speed is greatly increased compared with 2-DH models. The model is thus capable of processing large quantities of input wave and tidal data, making it suitable for the investigation of long-term processes on beaches and in nearshore regions. The model is designed to be used in conjunction with an appropriate sediment transport routine for problems concerned with longshore movement of sediment.

CONTENTS

CONTENTS (CONT/D)

1 INTRODUCTION

This report describes the theory, computational techniques and validation of a computational model for predicting wave and current conditions in nearshore regions. The model, known as the Nearshore Profile Model, uses the approximation of a straight coastline with parallel depth contours, and determines wave and current conditions at grid points along a profile line perpendicular to the coastline. The model has a number of new features:

1. It includes a modelling of tidal currents as well as wave-induced currents, with full interaction between the waves and the two types of current.

2. The theory is based on general mass, energy and momentum balance equations which are applicable both inside and outside the surf zone. The model can therefore be used for any profile length between offshore and the coastline, with no special treatment needed for the surf zone. The model can be used for any depth profile, and unlike some models is not restricted to monotonically decreasing depths.

3. Input to the model requires no special field exercise or additional numerical model study. Suitable input tidal conditions can be obtained from standard Tide Tables and Admiralty Charts. Input wave conditions are in the form of the representative wave height, period and direction at the offshore end of the profile line. These can be determined for instance by wave hindcasting from wind data. If measured wave or tidal data are available, these can provide a useful calibration of the model for a particular site, or if sufficiently extensive, an alternative source of input to the model.

4. The model can use tens or hundreds of thousands of input wave and tidal data values at a reasonable computing cost. This makes the model suitable for long-term predictions of hydrodynamic and morphological processes.

The report is structured as follows. Chapter 2 describes the background to the model, placing it in the context of alternative models and indicating the types of engineering problem to which it would be most suited. In Chapter 3 the program structure is described, and Chapters 4 and 5 give the details of the wave and current theory on which the model is based. Chapter 6 contains a comparison of values of wave height, wave set-up and wave-induced longshore currents predicted by the model against laboratory measurements. In Chapter 7 there is a comparison of model predictions of longshore tidal currents against field data. Finally, the main findings and conclusions are summarised in Chapter 8.

2 BACKGROUND

A range of computational modelling techniques is presently available for the prediction of inshore hydrodynamic conditions and morphological processes. Wave refraction models based on ray tracing over the coastal area of interest have been used for many years in coastal wave prediction problems. Early models of this type are described in Skovgaard et al (1975) and Abernethy and Gilbert (1975). More recent models, including the effects of currents on wave refraction are reported in Jonsson and Christofferson (1984), Southgate (1985) and Treloar (1986). Townend and Savell (1984) discuss the use of ray tracing models in present engineering practice.

These refraction models have often been combined with one-line beach plan shape models for the prediction of

erosion and accretion rates caused by the longshore drift of beach material. Examples of this type of model are described in Price et al (1972), Komar and Inman (1970) and Ozasa and Brampton (1980). A review of earlier work can be found in Le Mehaute and Soldate (1977), and a more recent assessment of the engineering uses of these models is given in Brampton and Motyka (1987).

The representation of physical processes in these models is very simplified with no tidal effects or wave-current interactive effects, meaning that site-specific calibration is required. Furthermore, wave-induced current and sediment transport quantities are calculated only as single average values across the surf zone (hence the name 'one-line'). However, because of their simplicity, one-line models are suitable for analysing large sequences of wave data and therefore for investigating long-term beach processes.

A considerable amount of research effort has been devoted to extending refraction models to incorporate other wave processes such as refraction by currents, diffraction, wave reflections, bottom friction, wave breaking and wind growth. Examples of these models are to be found in Booij (1981), Dalrymple et al (1984) and Booij et al (1985). Models have also been developed to analyse the transformation of wave spectra rather than waves with a single period and direction. Abernethy and Gilbert (1975), Booij et al (1985) and Treloar (1986) describe different approaches to the modelling of the transformation of wave spectra. Recently, sophisticated 2-D and 3-D models of the nearshore zone have been developed to analyse the interaction of waves, currents and sediment transport (eg Wind and Vreugdenhil (1986),

Stive and de Vriend (1987) and Yoo and O'Connor (1986)). Such types of model give detailed results of the hydrodynamic and morphological conditions, but have a high computing requirement which limits the number of input conditions that can be tested.

The Nearshore Profile Model described in this report is of intermediate complexity between the refraction/one-line models and the 2-D and 3-D nearshore models. The model incorporates most of the physical processes that are found in 2-D nearshore models, but restricts its modelling to a single profile line assuming a straight beach with parallel depth contours (Fig 1). This reduction to 1-D greatly increases the computational efficiency making the model capable of analysing the large number of input wave and tidal conditions (tens or hundreds of thousands of values) necessary for predicting long-term hydrodynamic and morphological processes.

3 PROGRAM STRUCTURE

The model is composed of a master program, separate wave and current modules and a number of auxiliary subroutines. The functions of these are described below.

3.1 Master Program

The master program reads all the data required by the model, such as depth values, sediment size values, and input wave and current conditions. These are converted into quantities required by the wave and current modules. The master program then makes alternate calls to these modules, starting with the current module, and passing updated values of current

and wave parameters between the two modules. These alternate calls are made up to a specified maximum number at which values of the wave and current parameters are expected to have converged. Results are output as a list of wave and current parameters at each point on the profile line for the input wave and tidal condition under study. If required, sediment transport calculations are then made. The master program returns to read in a new set of input conditions and the process is repeated until all the input conditions have been analysed.

3.2 Wave Module

The wave module determines values of wave parameters at each grid point for a single wave condition supplied at the offshore grid point. Values of current parameters at each grid point from the previous call to the current module are input to the wave module. These are used in the wave calculations but are not themselves altered by the wave calculations. At the end of the wave module, control is passed back to the master program.

3.3 Current Module

The current module determines values of current parameters at each grid point, using input tidal data from the master program and values of wave parameters from the previous call to the wave module. These wave parameters are unaltered in the current module. Control returns to the master program at the end of the module.

3.4 Auxiliary Subroutines

There are a number of auxiliary subroutines called from the wave and current modules to perform special

tasks, such as solving the wave-current dispersion relation (Eq 4.4.1) and determining enhanced friction factors using the method of O'Connor and Yoo (1988).

4 THEORY OF WAVE MODELLING

4.1 Introduction

The theory of wave and current modelling is described in the following two chapters. The model is fully interactive, with waves influencing the current field through seabed friction and the generation of longshore currents, and currents influencing the wave field through seabed friction and refraction. The techniques for modelling waves and currents will be described separately, but pointing out where the interaction occurs. The remainder of this chapter is devoted to wave modelling, and the following chapter is concerned with current modelling.

4.2 Incorporated wave processes

The processes affecting wave propagation incorporated in the model are shoaling, refraction (by depth variations and currents), seabed friction and wave breaking. In addition, wave radiation stresses are calculated which in turn form the basis for a calculation of wave-induced longshore currents and a set-up (or set-down) of the still water level. The radiation stresses which generate longshore currents are passed to the current module where the calculation of longshore currents takes place.

4.3 Input wave conditions

Input wave conditions are supplied at the grid point furthest offshore. These take the form of a height, period and direction of a single-period and

single-direction wave. If this wave is regarded as representative of a spectrum, the input conditions should be representative spectral quantities (such as significant or root-mean-square wave height, peak or median period, and mean direction). A tide level is also input and this is assumed constant for all the grid points. Values of the longshore current velocities determined from the previous call to the current module are input at each grid point. The model is re-run at different tidal levels to determine wave conditions at different states of the tide.

4.4 Wave kinematics

Wave kinematics refers to the determination of wave direction and wave celerity (ie phase velocity) and their derived quantities. When (as in the present model) refraction by currents as well as by depth variations occurs, it is necessary to make the distinction between wave orthogonals and wave rays (Fig 2). A wave orthogonal is a line drawn perpendicular to the wave crest, while a wave ray is a line drawn in the direction of travel of wave energy. In the absence of currents, the wave orthogonals and rays are identical, but with currents present the two are generally different. A further distinction has to be made between quantities measured relative to the seabed (referred to as 'absolute' and denoted by a subscript 'a') and those measured relative to an observer travelling with the current (referred to as 'relative' and denoted by a subscript 'r').

The fundamental equation to be solved at each grid point is the dispersion relation in the presence of currents:

$$(\omega_a - Uk\ \mathrm{Cos}(\delta-\alpha))^2 = gk\ \tanh kh \qquad 4.4.1$$

in which ω_a is the absolute wave angular frequency

(=2π/period), U is the current velocity, δ is the angle between the current direction and the onshore direction (Fig 2), α is the angle between the wave orthogonal and the onshore direction (Fig 2), g is the acceleration due to gravity, h is the water depth, and k is the wavenumber. Equation 4.4.1 is solved for k using a Newton-Raphson iteration technique. This is carried out in an auxiliary subroutine called by the wave module. Once k has been calculated, the following related quantities can be derived.

a) Relative wave angular frequency

$$\omega_r = \omega_a - Uk \cos\alpha \qquad 4.4.2$$

b) Relative wave celerity

$$c_r = \frac{\omega_r}{k} \qquad 4.4.3$$

c) Relative group velocity

$$c_{gr} = \frac{\omega_r}{2k}\left(1 + \frac{2kh}{\sinh(2kh)}\right) \qquad 4.4.4$$

d) Absolute group velocity (the vector sum of U and c_{gr}. See Fig 2)

$$c_{ga} = \left(U^2 + c_{gr}^2 + 2Uc_{gr}\cos(\delta-\alpha)\right)^{\frac{1}{2}} \qquad 4.4.5$$

e) Ray direction (see Fig 2)

$$\mu = \tan^{-1}\left(\frac{U\sin\delta + c_{gr}\sin\alpha}{U\cos\delta + c_{gr}\cos\alpha}\right) \qquad 4.4.6$$

In order to derive wave kinematic quantities at the grid point under study (subscript i), given quantities

at the previous point (subscript o), Snell's law for the orthogonal direction is used:

$$\text{Sin } \alpha_i = \frac{k_o}{k_i} \text{ Sin } \alpha_o \qquad 4.4.7$$

This equation is then used with Equations 4.4.1-6 to predict the kinematic quantities at the point under study. A fuller discussion of wave-current refraction is given in Southgate (1985).

4.5 Wave dynamics: Energy balance equation

Determination of wave dynamics (ie wave height, wave energy and related quantities) is based on integration of the energy balance equation.

$$\frac{d}{dy}\left(\frac{E\, c_{ga}\, \text{Cos } \mu}{\omega_r}\right) = -\frac{(D_f + D_b)}{\omega_r} \qquad 4.5.1$$

in which y is the co-ordinate in the onshore direction (Fig 1), E is the wave energy density, and D_f and D_b are the (spatial) energy flux dissipation rates due to seabed friction and wave breaking respectively.

For linear waves, E is related to the wave height H by

$$E = \frac{1}{8} \rho g H^2 \qquad 4.5.2$$

in which ρ is the water density. Integration of Equation 4.5.1 provides the means of determining the wave height at a grid point in terms of quantities at the preceding point. In order carry out this integration, explicit expressions for D_f and D_b are

needed. Appropriate expressions are derived in the following two sections (4.6 and 4.7), and the method of integrating Equation 4.5.1 is described in Section 4.8.

4.6 Wave energy dissipation by seabed friction

The method used in the Nearshore Profile Model of determining seabed frictional dissipation is based on the boundary layer model of O'Connor and Yoo (1988) which in turn is an extension of work by Bijker (1966). This method takes into account fully the interaction of waves and currents with the seabed, and details of the method are reported in O'Connor and Yoo (1988), and Yoo (1986).

The first stage in this method is to relate the wave friction factor C'_{fw}, <u>without</u> current interaction, to the seabed roughness k_s. For sandy seabeds, k_s represents the height of the sand ripples rather than the dimensions of the individual sand grains. There exist a number of semi-empirical formulae relating C'_{fw} to k_s; the one used in the Nearshore Profile Model is that due to Kamphuis (1975), as modified by Swart (1974).

$$C'_{fw} = \exp\left[6.0(A_o/k_s)^{-0.23} - 6.96\right] \quad \text{No current interaction} \qquad 4.6.1$$

in which A_o is the semi-excursion length of the water particles at the seabed due to the oscillatory motion of the waves. According to small-amplitude linear wave theory, A_o is related to the wave height by

$$A_o = \frac{H}{2\ \mathrm{Sinh}\ (kh)} \qquad 4.6.2$$

Equation 4.6.1 provides the starting point in O'Connor

and Yoo's method for determining a value of C_{fw} in which interaction between waves and currents is taken into account.

One result of this method is that the interacted frictional dissipation manifests itself only through an enhancement of the separate wave and current friction factors. This property allows wave and current energy dissipation rates to be treated independently. According to O'Connor and Yoo, the wave energy dissipation rate is given by:

$$D_f = \rho C_{fw} V_o^3 \qquad 4.6.3$$

in which C_{fw} is the wave friction factor enhanced by interaction with currents, and V_o is the maximum wave orbital velocity at the seabed. For linear waves V_o is related to the wave height by

$$V_o = \frac{H \omega_r}{2 \sinh (kh)} \qquad 4.6.4$$

In the model, C_{fw} is calculated at each grid point by the O'Connor and Yoo theory in auxiliary subroutines called by the wave module. Values of current parameters determined at the previous call to the current module are passed to these subroutines.

4.7 Wave energy dissipation by wave breaking

4.7.1 Introduction

There are many approaches to the problem of modelling the dissipation of energy in breaking waves, and a survey of these methods has been carried out in a companion report (Southgate (1988)). One of the tasks in the present study has been to investigate some of

these methods to discover the most accurate and suitable ones for the model. This investigation is described later in Chapter 6. In this section the theory of the adopted method will be described in some detail.

The method is based on Battjes and Janssen (1978) and is applicable to random waves. The formula used for the probability distribution of wave heights is,

$$P(H)\ dH = \frac{2H}{H^2_{rms}} \exp\ (-H^2/H^2_{rms})dH \qquad 4.7.1$$

and is known as the Rayleigh distribution. In this equation H is a general wave height, H_{rms} the root-mean-square wave height and P(H)dH is the probability of occurrence of a wave height lying in the range dH centred on H. The Rayleigh distribution has been derived theoretically under the assumptions of small-amplitude linear waves in deep water with a narrow frequency spectrum. Measurements in deep water have shown the Rayleigh distribution to be a good approximation. Even in shallow water, where the theoretical justification is less strong due to the distortions caused by shallow-water effects, measurements have shown the Rayleigh distribution still to be an adequate approximation for engineering prediction purposes (Thornton and Guza (1986)). However, in shallow water, the distribution needs to be truncated at the breaker wave height (ie the maximum height of waves allowed by the breaking process in shallow water). This is shown schematically in Figure 3.

The Battjes and Janssen method consists of three steps. Firstly, the breaker wave height is determined; secondly the probability of occurrence of broken waves using the truncated Rayleigh distribution

is found; and thirdly the rate of dissipation of energy in a broken wave is calculated.

4.7.2 Determination of breaker height

Battjes and Janssen use a modified form of an expression originally derived by Miche (1944).

$$H_b = \frac{0.88 \tanh(\gamma kh/0.88)}{k} \qquad 4.7.2$$

in which H_b is the breaker wave height, and γ is an empirically determined coefficient of the order of 0.8. A large number of simple empirically or theoretically derived formulas for H_b have been suggested. In this work, a modification of a widely-used empirical formula put forward by Weggel (1972) and recommended by the American Shore Protection Manual is used. The formula is,

$$H_b = \frac{ah}{1 + \frac{bh}{gT^2}} \qquad 4.7.3$$

in which

$$a = \frac{2a'}{1 + \exp(-19.5m)} \qquad 4.7.4$$

$$b = 43.75\,(1 - \exp(-19m)) \qquad 4.7.5$$

m is the beach slope and a' is an empirically determined parameter. In Weggel's original formula a' is set to 0.78. In the present work it was found necessary to increase the value of a' which has the effect of delaying the onset of breaking. The reasons for the choice of a' are discussed in Chapter 6.

4.7.3 Determination of the probability of broken waves

In Battjes and Janssen's method wave heights below H_b are assumed to be unaffected by the breaking process, while those above H_b are regarded as having broken. The probability of occurrence of a broken wave (Q) is therefore given by (Fig 3),

$$Q = \int_{H_b}^{\infty} P(H)\, dH$$

$$= \exp\left(-H_b^2/H_n^2\right) \qquad 4.7.6$$

in which H_n is the r.m.s wave height assuming no breaking. Of course H_n is not a physically realistic quantity, and it is required therefore to express Q in terms of H_{rms}, the actual r.m.s wave height (consisting of contributions from both broken and unbroken waves). In order to do this, some assumption has to be made about the probability distribution of the broken wave energy. Battjes and Janssen make the simple but physically plausible assumption that all broken waves have a wave height equal to H_b. This means that the probability distribution is truncated at H_b, but with an additional spike (in the sense of a Dirac delta function) at H_b representing the broken waves. H_{rms} can now be determined as the sum of unbroken and broken wave energy components,

$$H_{rms}^2 = \underbrace{\int_0^{H_b} H^2\, P(H)\, dH}_{\text{Unbroken}} + \underbrace{\int_{H_b}^{\infty} H_b^2\, P(H)\, dH}_{\text{Broken}}$$

$$= H_n^2 \left(1 - \exp\left(-H_b^2/H_n^2\right)\right) \qquad 4.7.7$$

H_n can be eliminated between Equations 4.7.6 and 4.7.7 enabling the probability of occurrence of broken waves (Q) to be expressed in terms of H_{rms} and H_b,

$$\frac{1 - Q}{(-\ln Q)} = \left(\frac{H_{rms}}{H_b}\right)^2 \qquad 4.7.8$$

This equation can be solved for Q by Newton-Raphson iteration. Having determined the probability of occurrence of broken waves, it is now necessary to determine the rate of energy dissipation in these waves.

4.7.4 Rate of energy dissipation in broken waves

In Battjes and Janssen's method, the rate of energy dissipation in a broken wave is estimated from the rate of energy dissipation in a tidal bore, a phenomenon similar in appearance to a broken wave. Battjes and Janssen derive the following expression for a broken wave,

$$D_b = \frac{\lambda \rho g^{3/2} k H^3}{8\pi h^{\frac{1}{2}}} \qquad 4.7.9$$

in which λ is an empirical constant of the order one which expresses the difference between the tidal bore and breaking wave processes. In a random sea, Equation 4.7.9 would apply to the case where all waves have broken. If only a proportion of the waves have broken, D_b needs to be multiplied by the probability of occurrence of a broken wave (Q), and H is set to the breaker height H_b,

$$D_b = \frac{\lambda \rho g^{3/2} k H_b^3 Q}{8\pi h^{\frac{1}{2}}} \qquad 4.7.10$$

Using Equation 4.7.8, D_b can be expressed in terms of

H_{rms},

$$D_b = \frac{\lambda \rho g^{3/2} k H_{rms}^3 f(Q)}{8\pi h^{\frac{1}{2}}} \qquad 4.7.11$$

where $f(Q) = Q\left(\frac{-1nQ}{1-Q}\right)^{3/2}$ 4.7.12

A graph of $f(Q)$ against H_{rms}/H_b is shown in Figure 4.

4.8 Integration of the energy balance equation

Explicit expressions for wave energy dissipation by bottom friction (Eq 4.6.3) and by wave breaking (Eq 4.7.11) have been obtained. It is now possible to integrate the energy balance equation (Eq 4.5.1) to determine how the wave height transforms as waves travel inshore.

Inserting the expressions for D_f and D_b into Equation 4.5.1 and using Equation 4.5.2,

$$\frac{1}{8}\rho g \frac{d}{dy}\left(\frac{H^2 c_{ga} \cos\mu}{\omega_r}\right) = -\frac{1}{\omega_r}\left[\frac{\rho C_{f\omega} \omega_r^3 H^3}{8 \sinh^3(kh)} + \frac{\lambda \rho g^{3/2} k H^3 f(Q)}{8 \pi h^{\frac{1}{2}}}\right] \qquad 4.8.1$$

in which for the expression for breaking waves, H is to be interpreted as H_{rms}. It can be seen that both D_f and D_b are proportional to H^3, a fact which allows a direct integration of Equation 4.8.1. D_b depends on H additionally through f(Q), although as Figure 4 shows, f(Q) is a regular monotonic function of H/H_b, thereby allowing a solution by iteration.

Rearranging Equation 4.8.1,

$$\frac{1}{H^3}\frac{d}{dy}\left(\frac{H^2 c_{ga} \cos\mu}{\omega_r}\right) = -\left[\frac{C_{fw}\,\omega_r^2}{g\,\sinh^3(kh)} + \frac{\lambda\, g^{\frac{1}{2}} k\, f(0)}{\pi\,\omega_r\, h^{\frac{1}{2}}}\right] \qquad 4.8.2$$

Using the identity,

$$\frac{1}{H^3}\frac{d}{dy}\left(\frac{H^2 c_{ga} \cos\mu}{\omega_r}\right) \equiv -2\left(\frac{c_{ga}\cos\mu}{\omega_r}\right)^{3/2}\frac{d}{dy}\left[\frac{1}{H}\left(\frac{\omega_r}{c_g \cos\mu}\right)^{\frac{1}{2}}\right] \qquad 4.8.3$$

Equation 4.8.2 can be written as,

$$\frac{d}{dy}\left[\frac{1}{H}\left(\frac{\omega_r}{c_{ga}\cos\mu}\right)^{\frac{1}{2}}\right] = \tfrac{1}{2}\left(\frac{\omega_r}{c_{ga}\cos\mu}\right)^{3/2}\left[\frac{C_{fw}\,\omega_r^2}{g\,\sinh^3(kh)} + \frac{\lambda\, g^{\frac{1}{2}} k\, f(0)}{\pi\,\omega_r\, h^{\frac{1}{2}}}\right] \qquad 4.8.4$$

Performing the integration between the previous grid point (subscript o) and the grid point under study (subscript i),

$$H_i = H_o K_s K_r K_d \left(\frac{1}{1+\beta H_o}\right) \qquad 4.8.5$$

where

$$K_s = \left(\frac{c_{gao}}{c_{gai}}\right)^{\frac{1}{2}} \quad \text{Shoaling coefficient} \qquad 4.8.6$$

$$K_r = \left(\frac{\cos\mu_o}{\cos\mu_i}\right)^{\frac{1}{2}} \quad \text{Refraction coefficient} \qquad 4.8.7$$

$$K_d = \left(\frac{\omega_{ri}}{\omega_{ro}}\right)^{\frac{1}{2}} \quad \text{Doppler coefficient} \qquad 4.8.8$$

$$\beta = \tfrac{1}{2}\left(\frac{c_{gao}\cos\mu_o}{\omega_{ro}}\right)^{\frac{1}{2}} \int_{y_o}^{y_i} \left(\frac{\omega_r}{c_{ga}\cos\mu}\right)^{\frac{3}{2}}\left[\frac{C_{fw}\,\omega_r^2}{g\,\sinh^3(kh)} + \frac{\lambda\, g^{\frac{1}{2}} k\, f(0)}{\pi\,\omega_r\, h^{\frac{1}{2}}}\right] dy \qquad 4.8.9$$

The integral in Equation 4.8.9 is evaluated at successive grid points by taking the average of the values of the integrand at y_o and y_i (ie the trapezium rule). Both C_{fw} and f(Q) are dependent on H, although relatively weakly. In the model an iterative procedure is used to calculate β using an initial estimate for H in the calculation of C_{fw} and f(Q) as

$$H = H_o K_s K_r K_d \qquad 4.8.10$$

In other words, the initial value of H is its value at the grid point under study assuming no dissipation. From Equations 4.8.5-9 a new value of H is calculated, which provides a closer approximation for C_{fw} and f(Q). Typically, three runs (two iterations) have been found to give convergence of H at all grid points to around 1% at worst.

4.9 Radiation stresses, wave set-up and longshore current generation

In general, waves exert a net momentum flux over a wave cycle in the direction of travel of the wave, as a result of their non-linear behaviour. This excess momentum flux, averaged over a wave cycle, is known as the wave radiation stress. When wave energy is dissipated, through seabed friction and breaking, some of this excess momentum flux is released from the wave and provides the driving force for other phenomena. Specifically, a set-up of the water level in the onshore direction, and the generation of a current in the longshore direction are caused by these spatial changes in the wave radiation stress.

Both of these phenomena are included in the model. The wave radiation stress in the onshore direction (S_{yy}) is given to second order in H by (Longuet-Higgins and Stewart (1964)),

$$S_{yy} = \frac{1}{8} \rho g H^2 \left[\left(\frac{2 c_{gr}}{c_r} - \frac{1}{2} \right) \cos^2\alpha + \left(\frac{c_{gr}}{c_r} - \frac{1}{2} \right) \sin^2\alpha \right] \qquad 4.9.1$$

The wave-induced set-up is calculated from the equation for momentum balance in the onshore direction.

$$\frac{d\eta}{dy} = - \frac{1}{\rho g \ (h+\eta)} \frac{dS_{yy}}{dy} \qquad 4.9.2$$

in which η is the wave-induced set-up of the still water level. η is determined at any grid point (subscript i) in terms of its value at the preceding grid point (subscript o) using a finite difference formulation of Equation 4.9.2

$$\frac{\eta_i - \eta_o}{\Delta y} = - \frac{1}{\rho g \ (h + (\eta_i + \eta_o)/2)} \frac{\Delta S_{yy}}{\Delta y} \qquad 4.9.3$$

Equation 4.9.3 is a quadratic in η_i with solution,

$$\eta_i = -h + \left[(h+\eta_o)^2 - \frac{2 \Delta S_{yy}}{\rho g} \right]^{\frac{1}{2}} \qquad 4.9.4$$

in which $\Delta S_{yy} = S_{yyi} - S_{yyo}$, $\Delta y = y_i - y_o$ and $h = (h_i + h_o)/2$.

Figures 14-19 show a comparison of computed and laboratory-measured values of set-up. It can be seen that there is a small set-down of the water level up to the breaker point (or, more strictly, the plunge point for plunging breakers, see Section 6.3) and a

larger set-up between the breaker point and the shoreline.

The wave radiation stress in the longshore direction, S_{xy}, is given to second order in H by (Longuet-Higgins (1970)),

$$S_{xy} = \frac{\rho g H^2 c_{gr} \text{Sin}2\alpha}{16 c_r} \qquad 4.9.5$$

The model uses spatial rates of change of S_{xy} to calculate the wave-induced longshore current. It is possible to calculate dS_{xy}/dy by a finite-difference approach similar to that used for wave set-up. However, it was noted by Longuet-Higgins (1970) that the irrotational part of S_{xy} remains unchanged by depth refraction and shoaling, and the only changes to S_{xy} arise from dissipative processes. For diffraction, and refraction by currents, S_{xy} does in general change, but not for the special case of a straight coastline with parallel depth contours considered in this model. Therefore the only changes to S_{xy} are those due to the dissipative processes of bottom friction and, principally, wave breaking. These points have been demonstrated quantitatively in Southgate (1987) where it was derived that,

$$S_{xyi} = \varepsilon^2 S_{xyo} \qquad 4.9.6$$

where ε is the ratio of the wave height at the inshore point calculated with dissipative processes to that calculated without dissipative processes. From Equation 4.8.5, ε is given by,

$$\varepsilon = \frac{1}{1 + \beta H_o} \qquad 4.9.7$$

The radiation stress gradient provides the driving force for the wave-induced current in the longshore direction. This driving force per unit sea area is given by,

$$F = - \frac{\partial S_{xy}}{\partial y} \qquad 4.9.8$$

Values of F at each grid point are passed to the current module where they are used to drive the longshore currents. The method employed for this is described in the following chapter.

5 THEORY OF CURRENT MODELLING

5.1 Incorporated current processes

Tidal and wave-induced currents in the longshore direction are determined in the model by solving the longshore momentum balance equation. The tidal currents are generated by longshore variations in the water-surface level (ie pressure-generated), and balanced by seabed friction and inertia. The wave-induced currents are generated by spatial gradients of the wave radiation stresses (see previous chapter), again balanced by seabed friction and inertia. Interaction between the two types of currents, and between them and the waves, is incorporated.

All currents are assumed to be depth-averaged and in the longshore direction. Therefore no onshore-offshore currents such as rip currents or undertow are modelled. Some quantities such as the maximum water surface elevation, ζ_m, are allowed a variation in the x-direction on a large length scale

(of the order of a tidal wavelength, typically about 500km), but locally they are regarded as constant in x. Wherever an x dependency is shown, the variation in x is understood to be on the large length scale. This assumption is consistent with the continuity (or mass conservation) equation

$$\frac{\partial}{\partial t}(h+\zeta) + \frac{\partial}{\partial x}\left[(h+\zeta)U \sin\delta\right] + \frac{\partial}{\partial y}\left[(h+\zeta)U \cos\delta\right] = 0 \qquad 5.1.1$$

at the local length scale.

5.2 Input current conditions

The driving forces for the tidal currents in the form of pressure gradients can be determined from standard data to be found in Tide Tables and Admiralty Charts for the locality under study (see Section 5.3.2). Alternatively, the driving forces can be calculated from measured current data (Section 5.7). These pressure-driven forces are assumed to be the same at all grid points. The wave radiation stresses which drive the wave-induced currents are passed to the current module from the previous call to the wave module (on the first call to the current module they are set to zero). Values of the seabed roughness are input at each grid point and are used to determine the current and wave friction factors.

5.3 Assumed form of current parameters. Symmetric tidal forces only

In the model, assumptions are made about the form of various parameters which affect the current field. Wherever expressions of the form exp(i...) appear, the real part only applies.

5.3.1 Surface elevation above mean sea level (ζ)

A general sinusoidal form is assumed with an angular frequency, ω, corresponding to the tidal cycle.

$$\zeta = \zeta_m (x) \exp(i[\omega t - \phi(x)]) \qquad 5.3.1$$

where t is time, ϕ is a general phase function, and ζ_m is the tidal amplitude. x is directed parallel to the coast (Fig 1). Note that ζ_m and ϕ are allowed to vary in the longshore direction because variations of these quantities take place on the large length scale.

5.3.2 Surface slope (S)

A general sinusoidal form is assumed.

$$S = S_m(x) \exp (i[\omega t - \Theta(x)]) \qquad 5.3.2$$

where S_m is the maximum surface slope and Θ is a general phase function. S is related to ζ through its definition.

$$S \equiv \frac{\partial \zeta}{\partial x} \qquad 5.3.3$$

Insertion of Equations 5.3.1 and 5.3.2 into Equation 5.3.3 yields the relationships between S_m, Θ and ζ_m, ϕ.

$$S_m^2 = (\frac{\partial \zeta_m}{\partial x})^2 + (\zeta_m \frac{\partial \phi}{\partial x})^2 \qquad 5.3.4$$

$$\Theta = \phi + \tan^{-1} [\frac{\zeta_m \partial \phi / \partial x}{\partial \zeta_m / \partial x}] \qquad 5.3.5$$

ϕ is chosen arbitrarily, usually being set to zero at high water. ζ_m, $\partial \zeta_m / \partial x$ and $\partial \phi / \partial x$ can be readily deduced from Tide Tables and Admiralty Charts. These are the input quantities which determine the pressure driving force for the tidal currents.

5.3.3 Longshore current velocity (U)

A general sinusoidal form is assumed.

$$U = U_m(x,y)\exp(i[\omega t - \psi(x,y)]) \qquad 5.3.6$$

in which U_m is the maximum tidal longshore current velocity and ψ is a general phase function. In this case, U is allowed to vary in the y-direction (along the profile line).

5.3.4 Shear stress at the seabed (τ)

The quadratic friction law is assumed.

$$\tau = \rho\, C'_{fc}\, U\, |U| \qquad 5.3.7$$

in which C'_{fc} is the current friction factor, without interaction with waves and τ is the seabed shear stress. In the Nearshore Profile Model, C'_{fc} is determined from Bijker's empirical formula (Bijker 1966),

$$C'_{fc} = 0.016\,(h/k_s)^{-1/3} \qquad 5.3.8$$

5.4 Solution of momentum balance equation. Symmetric tidal forces only

The longshore current is calculated from the solution to the momentum balance equation. This equation will be solved first for tidal currents alone and then for combined tidal and wave-induced currents.

The momentum balance equation for tidal currents alone is

$$\underset{\text{Inertia}}{\frac{\partial U}{\partial t}} + \underset{\text{Pressure Force}}{gS} + \underset{\text{Seabed Friction}}{\frac{\tau}{\rho h}} = 0 \qquad 5.4.1$$

These three terms represent the most important forces. Other effects such as Coriolis, lateral mixing and advection are usually much smaller in the nearshore zone. A linearising simplification to the expression for seabed friction is required. Equation 5.3.6 substituted into Equation 5.3.7 gives,

$$\tau = \rho\, C'_{fc}\, U_m^2 \exp\left(i(\omega t - \psi)\right) \left| \mathrm{Cos}(\omega t - \psi) \right| \qquad 5.4.2$$

In this simplification, the maximum value of the modulus is assumed at all times. τ will therefore be well predicted close to its maximum, and less well away from it. However, the most important effects of friction on current velocities occur around the maximum. The expression used for τ is therefore,

$$\tau = \rho\, C'_{fc}\, U_m^2 \exp\left(i(\omega t - \psi)\right) \qquad 5.4.3$$

Substitution of Equations 5.3.2, 5.3.6 and 5.4.3 into Equation 5.4.1 gives,

$$gS_m \exp\left(i(\omega t+\Theta)\right) + i\omega U_m \exp\left(i(\omega t-\psi)\right) + \frac{C'_{fc} U_m^2 \exp\left(i(\omega t-\psi)\right)}{h} = 0 \qquad 5.4.4$$

Equating amplitude and phase terms yields

$$g^2 S_m^2 = (\omega U_m)^2 + \left(\frac{C'_{fc}\, U_m^2}{h}\right)^2 \qquad 5.4.5$$

$$\text{and } \psi = \Theta - \tan^{-1}\left(\frac{\omega h}{-C'_{fc}\, U_m}\right) \qquad 5.4.6$$

Equation 5.4.5 can be written as a quadratic in U_m^2

with solution,

$$U_m = \frac{1}{\sqrt{2}} \left(\frac{\omega h}{C'_{fc}}\right) \left[\left(1 + \frac{4\, g^2\, S_m^2\, C'^2_{fc}}{h^2\, \omega^4}\right)^{\frac{1}{2}} - 1\right]^{\frac{1}{2}} \qquad 5.4.7$$

ϕ can then be found from Equation 5.4.6 using the value of U_m from Equation 5.4.7. It can be seen that different values of U_m and ϕ will be obtained at different grid points through the influence of the depth (h) and current friction factor (C'_{fc}). Equations 5.4.6 and 5.4.7 have been used to predict tidal flows in the Dover Strait with qualitative agreement with measurements (R L Soulsby, private communication). More detailed comparisons with measured data at Aberdeen are presented in Chapter 7 of this report.

5.5 Assumed form of current parameters. General tidal and wave-induced forces

The following assumptions are made about the form of the parameters which determine the current field.

5.5.1 Surface elevation above mean sea level (ζ)

A general sinusoidal form identical to Equation 5.3.1 is assumed, with an additional term $\zeta_o(x)$ on the right-hand side.

5.5.2 Surface slope (S)

A general sinusoidal form is assumed as in Equation 5.3.2 but with a constant (in time) offset to account for any asymmetry in the pressure driving force.

$$S = S_m(x)\, \exp\left(i\left[\omega t - \Theta(x)\right]\right) + S_o(x) \qquad 5.5.1$$

The values of S_m and Θ are given by Equations 5.3.4 and 5.3.5. S_o is an input parameter. It can be expressed in terms of a deep-water time-independent tidal current which is a quantity that can be more readily measured or deduced from information contained in Admiralty Charts. This is considered in Section 5.7.

5.5.3 Longshore current velocity (U)

A general sinusoidal form is assumed as in Equation 5.3.6 but with a time-independent current, U_o, to represent the steady tidal current and (quasi-) steady wave-induced current.

$$U = U_m(x,y)\exp(i[\omega t-\psi(x,y)]) + U_o(x,y) \qquad 5.5.2$$

It is assumed that the wave-induced current remains steady (apart from random fluctuations) over several hours, the time period during which significant changes to tidal currents take place. Wave-induced currents will, of course, vary over a longer timescale, hence they are termed "quasi-steady".

5.5.4 Shear stress at the seabed (τ)

The quadratic friction law, Equation 5.3.7, is used for τ, but with U given by Equation 5.5.2. Substituting Equation 5.5.2 into Equation 5.3.7 gives

$$\tau=\rho\, C_{fc}\left(U_m\exp(i[\omega t-\psi])+U_o\right)\left|U_m\cos(\omega t-\psi)+U_o\right| \qquad 5.5.3$$

C_{fc} is the current friction factor, including wave interaction, and is determined by the O'Connor and Yoo method. Equation 5.5.3 is then linearised by taking the maximum value of the modulus and assuming that this holds throughout the tidal cycle.

$$\tau = \rho C_{fc} \left(U_m \exp(i[\omega t-\psi]) + U_o\right) \left(U_m + |U_o|\right) \qquad 5.5.4$$

τ can be written as the sum of time-dependent (τ_{td}) and time-independent (τ_{ti}) terms.

$$\tau_{td} = \rho C_{fc} U_m \left(U_m + |U_o|\right) \exp\left(i[\omega t - \psi]\right) \qquad 5.5.5$$

$$\tau_{ti} = \rho C_{fc} U_o \left(U_m + |U_o|\right) \qquad 5.5.6$$

5.6 Solution of momentum balance equation. General tidal and wave-induced forces

The momentum balance equation for tidal and wave-induced currents is

$$\underset{\text{Inertia}}{\frac{\partial U}{\partial t}} + \underset{\substack{\text{Pressure}\\ \text{Force}}}{gS} + \underset{\substack{\text{Seabed}\\ \text{Friction}}}{\frac{\tau}{\rho h}} = \underset{\substack{\text{Wave Radiation}\\ \text{Stress}}}{\frac{F}{\rho h}} \qquad 5.6.1$$

F is given by Equation 4.9.8, and is passed to the current module from the previous call to the wave module. On the first call to the current module F is set to zero. Ouasi-steady driving forces from other sources, such as wind stress, could be included on the right-hand size of Equation 5.6.1. These are not considered in this report but represent a possible extension of the model.

The solution of the momentum balance equation is found by substituting Equations 5.5.1, 5.5.2 and 5.5.4 into Equation 5.6.1, and equating time-independent and time-dependent parts,

$$gS_m \exp(i[\omega t-\Theta]) + i\omega U_m \exp(i[\omega t-\phi])$$

$$+ \frac{C_{fc} U_m (U_m+|U_o|)\exp(i[\omega t-\phi])}{h} = 0 \qquad 5.6.2$$

and $$\rho\, C_{fc}\, U_o(U_m + |U_o|) = F - \rho g h S_o \qquad 5.6.3$$

Equating the amplitude and phase parts of Equation 5.6.2 yields,

$$g^2 S_m^2 = \omega^2\, U_m^2 + \left(\frac{C_{fc}\, U_m (U_m+|U_o|)}{h}\right)^2 \qquad 5.6.4$$

and $$\phi = \Theta + \tan^{-1}\left[\frac{-\omega h}{-C_{fc}(U_m+|U_o|)}\right] \qquad 5.6.5$$

Equations 5.6.3 and 5.6.4 are coupled expressions for the two unknowns, U_m and U_o. ϕ is found from Equation 5.6.5 once U_m and U_o are known.

Solutions for U_m and U_o can be efficiently determined using a Newton-Raphson iteration technique. Equations 5.6.3 and 5.6.4 are written in the form,

$$U_o = \frac{Gh}{C_{fc} q} \qquad 5.6.6$$

and

$$U_m = \frac{gS_m h}{(h^2\omega^2 + C_{fc}^2\, q^2)^{\frac{1}{2}}} \qquad 5.6.7$$

where $$G = \frac{F}{\rho h} - gS_o \qquad 5.6.8$$

and $$q = U_m + |U_o| \qquad 5.6.9$$

Adding Equations 5.6.6 and 5.6.7,

$$q = \frac{|G|\,h}{C_{fc}\,q} + \frac{gS_m h}{(h^2\omega^2 + C_{fc}^2 q^2)^{\frac{1}{2}}} \qquad 5.6.10$$

Rewriting Equation 5.6.10,

$$f(q) \equiv (q - \frac{|G|\,h}{C_{fc}\,q})^2 \,(h^2\omega^2 + C_{fc}^2 q^2) - g^2 S_m^2 h^2 = 0 \qquad 5.6.11$$

Differentiating,

$$f'(q) = 2(q - \frac{|G|\,h}{C_{fc}\,q})(1 + \frac{|G|\,h}{C_{fc}\,q^2})(h^2\omega^2 + C_{fc}^2 q^2) + 2q\,C_{fc}^2\,(q - \frac{|G|\,h}{C_{fc}\,q})^2$$

Simplifying,

$$f'(q) = 2(1 - \frac{|G|\,h}{C_{fc}\,q})[h^2\omega^2 + 2C_{fc}^2 q^2 + \frac{|G|\,h^3\omega^2}{C_{fc}\,q^2}] \qquad 5.6.12$$

Successive approximations to the solution of Equation 5.6.11 for q are made using the formula,

$$q_{j+1} = q_j - \frac{f(q_j)}{f'(q_j)} \qquad 5.6.13$$

where the subscript j denotes the jth approximation. Some care has to be given to the initial estimate for q. Figure 5 shows a graph of f(q) against q and indicates that there are two roots to Equation 5.6.11 either side of a minimum value of f(q) determined by setting f'(q) to zero. The minimum f(q) and the corresponding value of q are,

$$f(q)_{min} = -g^2 S_m^2 h^2 \qquad 5.6.14$$

$$q_{min} = (\frac{|G|\,h}{C_{fc}})^{\frac{1}{2}} \qquad 5.6.15$$

From Equations 5.6.6, 5.6.15 and the definition of q (Eq 5.6.9),

$$q^2 - q_{min}^2 = qU_m \qquad 5.6.16$$

Since all quantities in Equations 5.6.16 are positive, it follows that q is greater than q_{min}, and therefore that the higher of the two roots to the solution of Equation 5.6.11 is the correct root. Convergence to this root can be assured by taking the initial estimate for q to be greater than q_{min}. This is done as follows: It is noted that the expression for q_{min}, Equation 5.6.15, is the same as the solution for $|U_o|_{min}$ in the absence of interaction with tidal-oscillatory currents (Eqs 5.6.6 and 5.6.9 are solved for $|U_o|$ with U_m set to zero). The initial estimate for q used in this model uses the sum of q_{min} and the solution for U_m in the absence of steady currents (Eq 5.4.7). The initial estimate for q is thus taken as the sum of the solutions for the steady and oscillatory currents in the absence of interaction between the two. This initial estimate will always be greater than q_{min} and ensures convergence to the correct solution for q.

5.7 Use of measured current data as input to the model

In Section 5.3, it was described how the tidal pressure forces, required as input to the model, could be calculated from quantities that could be readily derived from Tide Tables and Admiralty Charts. It is envisaged that this method is used if there are no reliable tidal current velocity data available at the site of interest. If such data are available, they can be used as an alternative method for deriving the input tidal pressure forces. Generally, this method

would be preferred, since it is based on actual site measurements.

The required data are:

a) A series of measurements of longshore current velocity at a point on or close to the profile line outside the surf zone.

b) The corresponding times, relative to High Water, at which the measurements were made.

c) The average depth of water at the site of the measurements.

The aim is to fit a sinusoidal curve to the data, with period equal to the tidal period and with a constant vertical offset. This can be achieved using a three-parameter least-squares analysis to give U_m, U_o and ϕ. These are then used to calculate the parameters determining the tidal pressure driving force, namely S_m, S_o and Θ, using Equations 5.6.3, 5.6.4 and 5.6.5. If the measurement point is well outside the surf zone, it can be assumed that the influence of wave-induced currents is small, and average to zero when a long sequence of tidal current velocity data is considered. Therefore F can be set to zero in Equation 5.6.3. Having determined S_m, S_o and Θ, these values are assumed to apply at all points along the profile line. If there is a large spring-neap range, it will be necessary to group the data into bands at intervals through the range, and carry out separate analyses for each band.

6 COMPARISON OF THE NEARSHORE PROFILE MODEL WITH LABORATORY DATA

6.1 Introduction

As a first stage in the verification of the Nearshore Profile Model, comparisons between model predictions and laboratory measurements have been carried out. Unfortunately, no suitable laboratory experiments appear to have been carried out in which both tidal-oscillatory and steady currents, as well as waves, are simulated. However, a number of experimental investigations have been reported in the technical literature in which waves and the wave-induced steady currents are measured. Most of these investigations have used the 1-D approximation for which the Nearshore Profile Model is applicable; namely a straight beach with parallel depth contours. Such laboratory studies would therefore be applicable in verifying the modelling of waves and their interaction with wave-induced currents, although the omission of tidal-oscillatory currents means that the full scope of the model would not be tested. Nevertheless, comparisons with laboratory data would provide a valuable first stage in the verification of the model, and will also allow comparisons with alternative numerical models in which the effects of tidal-oscillatory currents are not incorporated.

The laboratory measurements selected for this comparison were those by Visser (1982, 1984a and 1984b) carried out at Delft University of Technology, Holland. Visser's model consisted of a straight beach with a regular seaward bed slope. Mono-period and mono-directional waves were used, and measurements were made of wave height, wave-induced set-up of the still water level, and wave-induced longshore

currents. Other experimenters have performed laboratory studies under similar conditions, but Visser's investigation appears to have been carried out particularly carefully, most notably in preventing "end effects" from contaminating the longshore currents. Other researchers have also used the Visser measurements for comparison with their own numerical models (Yoo and O'Connor (1987), Pechon (1987), Bonneton and Gaillard (1985) and Visser's own model (1984a and b)) and therefore a comparison of the Nearshore Profile Model with these alternative models is possible.

6.2 Experimental arrangement, procedures and results

The experimental arrangement is shown in Figure 6. A snake-type wave generator, capable of producing regular waves at a specified direction, was situated at one end of the wave basin. Opposite the generator, smooth concrete beaches were constructed with regular slopes of 1 in 10 and 1 in 20 respectively. For the final experiment the 1 in 20 slope was roughed by bonding gravel, with dimensions between 5 and 9mm, on to the concrete. Wave-guide walls were installed across the basin at the angle of the initial wave direction.

A circulation system to maintain currents along the beach was constructed using a Rehbock weir and pump. On the upstream wave guide a distribution system was built to ensure that the recirculated flow matched the wave-induced flows at all points along the beach profile. Details of these experimental arrangements are given in Visser (1982). The techniques and procedures for measuring the various wave and current

parameters are described in detail in Visser's reports.

Seven experiments were carried out in total, three with the 1 in 10 slope, three with the 1 in 20 slope, and one with the roughened 1 in 20 slope. Each experiment used a different incident wave height, period and direction. Wave and current parameters were measured at regular intervals in the shore-normal direction for up to five sections, shown in Fig 6. Averaged quantities across these sections were then calculated. Table 1 lists the incident conditions and averaged inshore results for all seven experiments.

6.3 Comparison between experimental results and model predictions

The seven experiments were reproduced in the Nearshore Profile Model using a grid spacing of 0.1m for the 1 in 10 slope and 0.2m for the 1 in 20 slope. A range of model tests was carried out to determine the optimum values of the three empirically-determined parameters: the bed roughness k_s (which determines the wave and current friction factors), the breaking dissipation factor λ, and the breaker height factor a'. It was assumed initially that the same values of these parameters would apply for the three tests with the 1 in 10 slope, and a different set of values for the 1 in 20 slope tests. It so happened that values of λ and a' turned out to be the same for all the tests, a finding that would be expected since the effect of the different bed slopes on wave breaking had already been explicitly incorporated via Eqs 4.7.3, 4.7.4 and 4.7.5. Different values of k_s were found for the two sets of experiments, a result again to be expected since the beach slope was completely remoulded for the second set. In optimising the

values of k_s, λ and a', the best fits over each set-of-three experiments for longshore current velocities, wave height and wave set-up over the whole profile length were determined.

It was found that none of these quantities were particularly sensitive to the value of λ. Accordingly the value of λ was set to one, and the breaking processes was fitted through changing the value of a'. This parameter had a clear effect; increasing the value of a' resulted in wave breaking occurring nearer to the shoreline, and with a more rapid (spatial) rate of decrease of wave energy once breaking had started. The values of k_s were estimated by Visser to be about 0.001m for the concrete slopes and 0.01m for the gravel-roughened slope. However, these values are approximate, and the value of k_s was chosen to give a best-fit to the data, but ensuring that the chosen values were not greatly different from the estimated values. Longshore current velocities were quite sensitive to the value of k_s whereas the wave height and wave set-up were relatively insensitive, indicating that the choice of k_s is more important in determining current rather than wave properties.

The following table summarises the values of k_s, λ and a' used to give a best-fit to the experimental data.

Empirical parameter	Best-fit value in model		
	1 in 10 slope	1 in 20 slope	1 in 20 slope, roughened
k_s	0.002m	0.0006m	0.01m
λ	1	1	1
a'	1.18	1.18	1.18

In Visser's own mathematical model, he used best-fit values for k_s of 0.0015m for the 1 in 10 slope, 0.0008m for the 1 in 20 slope, and 0.015m for the roughened 1 in 20 slope.

The results of the comparisons are shown in Figs 7-13 for longshore currents, Figs 14-19 for wave set-up, and Figs 20-25 for wave heights. Insufficient experimental data were available for comparing wave set-up and wave height for experiment 7, with the roughened bed slope. All the figures show good agreement, comparable to that of alternative numerical models. These results are discussed in Section 6.5.

6.4 Further tests with the Nearshore Profile Model

The Nearshore Profile Model results presented so far have included simulation of the breaking of random waves. It is of interest to demonstrate the differences that would occur if the breaking of single period/direction waves were included instead. This can be achieved in the model by setting the coefficient λ initially to zero (corresponding to no breaking) and maintaining it at this value until the

wave height exceeds the breaker height. At this point λ and f(Q) are set to one, corresponding to full breaking, and these values are maintained as far as the shoreline.

Figs 26-28 show respectively the longshore current, wave set-up and wave height with a breaking factor a'=1.18 for both random and single period/direction breaking waves. It can be seen from Fig 26 that there is a very sharp gradient of the longshore current velocity at the plunge point in the single period/direction case, and the peak velocity is somewhat higher than for random wave breaking. Further shorewards there is a regular decay of current velocity, while further seawards there is a small current velocity resulting from wave energy dissipation by seabed friction. In Fig 27, showing the wave set-up, there is a larger set-down at the plunge point, while values shorewards are similar. The comparison with wave height, shown in Fig 28, again indicates a higher peak at the plunge point, although in this case of course, both model peaks are shorewards of the experimental peak at the breaker point. The overall conclusion is that model results based on single period/direction wave breaking gives noticeably poorer agreement with the experimental measurements compared with model results using random wave breaking.

It is also of interest to investigate the effect of altering the breaking factor a'. Figs 29-31 show a comparison between experimental measurements, and model tests with random and single period/direction wave breaking using a breaking factor a'=0.78 (the commonly used value for tuning to the breaker line, see Section 6.5). These figures therefore show results for the same tests discussed in the previous paragraph (Figs 26-28) but with the breaking factor tuned to the breaker line rather than the plunge line.

Comparing the two sets of figures, it can be seen that the predictions of longshore current velocities (Figs 26 and 29) are poorer with a'=0.78, the peak occurring too far seawards. A similar comparison is seen for wave set-up (Figs 27 and 30) with the maximum set-down again occurring too far seawards for a'=0.78. The comparison for wave height (Figs 28 and 31) indicates much better agreement for a'=0.78, particularly in the decay of wave height shorewards of the breaker line. Wave heights at the breaker line itself are still underpredicted, probably due to the absence of any modelling of non-linear waves (Section 6.5).

6.5 Discussion

An important finding from Visser's experiments was that the wave set-up and wave-induced longshore currents did not start their strong increase at the breaker line (where maximum wave height occurs, immediately before breaking) but at the plunge line (where the plunging breaker strikes the still water). There is a significant distance between these two lines, of the order of $\frac{1}{4}$ to $\frac{1}{2}$ of the entire width of the surf zone, during which the wave height decreases rapidly as the crest curls over, but the water motion remains essentially irrotational and the excess momentum flux is not released from the waves.

In the Nearshore Profile Model, and other computational models of a similar type, the radiation stresses are determined from the wave heights, and thus radiation-stress-related quantities such as wave set-up and wave-induced longshore currents appear to start at the breaker line. To overcome this problem some researchers such as Visser (1984a and b) and Svendsen (1984) have developed theories which explicitly incorporate the breaker-line to plunge-line distance or related quantities. Models based on these theories require this distance to be input as a measured and pre-determined quantity. Whilst this is possible in the comparison with Visser's experiments,

since this quantity was measured, such information would not be available in general applications and would render such an approach of little use as a predictive tool. It may be possible, on the basis of large numbers of observations and measurements of breaking waves, to relate the breaker line/plunge line distance to the breaker type (plunging, spilling etc) and determinable quantities of the waves just before breaking (height, steepness etc), but a study of this sort has yet to be carried out, and in any event is likely to be subject to considerable uncertainties. Nevertheless such a study could be useful for modelling long sequences of waves which involve a mixture of breaker types.

The method used in the Nearshore Profile Model to deal with this problem is to "tune" the breaking process so that waves appear to break either at the breaker point or the plunge point. The idea is that if wave quantities are of principal interest in a particular application the model would be tuned to the breaker line, whereas if radiation-stress-related quantities (wave set-up, longshore currents) are of principal interest the model would be tuned to the plunge line. A number of approaches for achieving this tuning were tried, and it was found that the onset of breaking could be made to occur nearer to the shoreline by increasing the value of a' in the breaker height criterion, Eq 4.7.4. The model results presented in Figs 7-28 were tuned to the plunge line using a value of a'=1.18, somewhat larger than the usually used value of 0.78 for tuning to the breaker line (Figs 29-31).

Wave set-up and wave-induced longshore currents are shown to be accurately predicted in the figures with a' = 1.18, but as expected there is less accuracy in the wave height predictions. In fact, the mis-tuning of the breaking process is not the only source of

error; the assumption of random waves for the breaking process in the model (whereas regular waves were used in the experiments) will tend to depress wave heights at the breaker point, and cause a less rapid wave height decay in the surf zone, as indicated in the figures. A further discrepancy is caused by the absence of any modelling of non-linear processes which are important close to and during the breaking process, and cause a greater peaking of wave height just before breaking. Some idea of the relative importance of these contributions to the error in wave height at the breaker line can be seen by comparing wave heights from the Nearshore Profile Model run separately with random waves and single period/direction waves (Section 6.4), and also with results from two models used by Pechon (1987) incorporating linear and non-linear (Serre theory) single period/direction waves respectively.

Computational Model	Wave height at Breaker Line (Test one) cm	% Difference from Measured Wave Heights
Measurement	10.5	-
NPM linear random waves	8.7	-17.1%
NPM linear single period/direction waves	9.7	-7.6%
Pechon linear single period/direction waves	9.1	-13.3%
Pechon non-linear single period/direction waves	10.8	+2.9%

Another feature to be commented on is the method of modelling wave-induced longshore currents in the Nearshore Profile Model. For single period/direction waves, lateral diffusion due to turbulence within the surf zone plays an important part in determining the distribution of longshore currents along the profile line. Without the effects of lateral diffusion, a very sharp cutoff at the plunge line will be obtained (Fig 26). Inclusion of lateral diffusion smooths over this discontinuity and gives a significant longshore current seawards of the plunge line. In the Nearshore Profile Model, however, lateral diffusion is not incorporated as this would considerably increase the complexity of modelling longshore currents beyond the analytical forms obtained in Chapter 5. Furthermore, an additional empirically-determined parameter, the eddy viscosity coefficient, would need to be introduced. Instead, the distribution of longshore currents is obtained by modelling the breaking of random waves. The probability distribution of wave heights in random waves implies that the breaker and plunge lines are 'smeared out' in the shore-normal direction, thereby creating a distribution of longshore currents similar to that obtained with mono-frequency waves and lateral diffusion.

It has been found by other researchers that the inclusion of lateral diffusion in a predictive model will make only a small difference to the longshore current distribution, negligible for the purpose of engineering predictions, provided that random wave breaking is simulated in the model (Battjes (1972), Thornton and Guza (1986)). The good agreement between the model predictions and experimental measurements in the present study (Figs 7-13) bears out this conclusion.

7 COMPARISON OF THE NEARSHORE PROFILE MODEL WITH FIELD DATA

7.1 Introduction

The comparison of the Nearshore Profile Model with laboratory experiments, described in the previous chapter, was for the case of waves and wave-induced currents only. No suitable laboratory simulation of wave and tidal current effects appears to have been carried out. In order to test the model's ability to predict tidal currents, and their interaction with waves and wave-induced currents, comparisons with field data measured at suitable coastal sites are required.

Again, there is a problem of obtaining an adequate field data set. The site should be a fairly long, straight stretch of coastline with a regular seabed bathymetry and where there is a large tidal range. Measurements should ideally consist of a set of longshore current velocity values at spatial intervals along a shore-normal line within and outside the surf zone, and at regular time intervals during the tidal cycle. Simultaneous wave measurements should be made, and the longshore current measurements should be repeated under different wave conditions. Although a number of suitable sites exist around the British and NW European coastlines, the detailed measurements needed to obtain a sufficiently large database for a thorough testing of the model mean that such a field exercise would be a major undertaking.

A survey of presently available data sets has not revealed one suitable for testing the full scope of the Nearshore Profile Model. However, because of the difficulty in obtaining details of field studies

carried out by many different institutions in different countries, this survey is by no means exhaustive. On present information, it seems that field studies at suitable sites in NW Europe do not have sufficiently detailed series of longshore current measurements. Larger studies have been carried out in the USA and Canada, but these have been in environments where tidal currents were weak, and were regarded as negligible in the subsequent analyses of the field data. It appears that a major field exercise of comparable detail to the American exercises but appropriate to British and NW European coastal environments would be a valuable, although costly, undertaking.

In the absence at the present time of a comprehensive field exercise, the Nearshore Profile Model has been compared with a smaller series of field measurements made at a coastal site immediately to the north of Aberdeen harbour in Scotland. These measurements consisted of float-tracking at a number of points on a shore-normal line to measure longshore current velocities. As conditions were calm, tidal currents only were measured. This study is described in the following section.

7.2 Field measurements at Aberdeen and comparison with model predictions

In the Spring of 1987, Hydraulics Research Ltd carried out a field measurement exercise in the area around Aberdeen Harbour. As part of this exercise, current velocities were measured using float-tracking drogues released from five points on a shore-normal line just to the north of the harbour (Fig 32). The coastline north of Aberdeen is long and straight with a regular seabed slope out to deep water, making it a good site

at which to test the Nearshore Profile Model. The drogue-release points were, however, sufficiently close to the harbour for north-flowing tidal currents to be significantly distorted by the harbour and the headland immediately to the south of the harbour, Girdle Ness. Accordingly, measurements were made only on the south-flowing tide. These measurements consisted of the releasing and tracking of drogues from each release-point on three separate occasions during the south-flowing tide.

The Nearshore Profile Model was set up with 41 grid points extending from deep water (50m CD) to the top of the beach. The grid points were not evenly spaced being more concentrated nearer the coast. Since conditions were calm with very little wave action during the float-tracking exercise, the model was run to determine tidal currents only, with no waves. Tidal currents were predicted at 20 stages during a semi-diurnal tidal cycle for each drogue-release point.

The tidal quantities needed for input to the model (see Section 5.3.2) were deduced from information on tidal elevations and phases published in tide tables for ports along the Aberdeen coastline between Peterhead and Dundee. Sediment samples from the site indicated a seabed composed predominantly of fine to medium sand (about 200 microns). Accordingly k_s was set to a value appropriate to a typical ripple height for this type of sand, of 0.016m. In this comparison with field data, the model was used as a predictive tool; no adjustments were made to the input parameters to obtain a best fit.

The comparison between the measured longshore tidal current velocities and the model predictions is shown in Fig 33. The full lines represent the model tidal

curves, and the large symbols represent the measured current velocities. It can be seen that two of the three sets of measurements (at approximately HW-5½hrs and HW-½hr) show very good agreement with the model predictions, particularly in determining the relative phases of the current velocities at the different drogue-release points. The third set, close to the maximum predicted southerly currents, shows that the model considerably over-predicts at the smaller depths. It is probable that these strong southerly currents were deflected seawards by being close to the harbour, and charts of the drogue paths showed that this was so. Generally, therefore, the agreement between the model predictions and measurements is good.

In the previous chapter, the Nearshore Profile Model was shown to compare well with laboratory measurements of waves and wave-induced currents. In the present chapter, a comparison with field measurements of tidal currents has shown promising results. The next stage is to compare the model with measurements incorporating the interaction between waves, wave-induced currents and tidal currents. Such a comparison needs to await a sufficiently comprehensive field measurement exercise at a suitable coastal site.

8 SUMMARY AND CONCLUSIONS

1) A computational model, known as the Nearshore Profile Model, for predicting wave and current conditions in nearshore regions is described in this report.

2) The model uses the approximation of a straight coastline with parallel depth contours, and determines wave and longshore current conditions

along a profile line perpendicular to the coastline. The new features incorporated in the model are

a) A modelling of tidal as well as wave-induced currents, with full interaction between the waves and the two types of current.

b) A theory based on general mass, energy and momentum balance equations, which is applicable both inside and outside the surf zone.

c) Input conditions which require no special field measurement exercise or additional numerical model study. If measurements are available, they will provide a useful calibration of the model at a particular site, or an alternative method of input.

d) A theoretical framework and efficient computational algorithm which allow tens or even hundreds of thousands of input wave and tidal conditions to be analysed at reasonable cost. This makes the model suitable for long-term predictions of hydrodynamic and morphological processes.

3) The program is structured with separate wave and current modules. The model is made interactive by allowing information to be exchanged between these modules. The program makes alternate calls to these modules up to a specified maximum number of times at which values of the wave and current parameters are expected to have converged.

4) Wave transformation between offshore and inshore points is based on the wave energy balance

equation. The physical processes incorporated are shoaling, refraction (by depth variations and currents), seabed friction and wave breaking. Currents affect the wave field through refraction and seabed friction. Wave radiation stresses, which cause a set-up of the still water level and the generation of longshore currents, are also calculated.

5) Currents are assumed to be depth-averaged and in the longshore direction, and are determined from the equation of momentum balance. The tidal currents are generated by longshore variations in the water-surface level (ie pressure-generated), and balanced by seabed friction and inertia. The wave-induced currents are generated by spatial gradients of the wave radiation stresses, again balanced by seabed friction and inertia. Interaction between the two types of current occurs, and between them and the waves. Waves influence the current field through seabed friction and the generation of longshore currents.

6) The model has been compared with laboratory measurements in which waves and wave-induced currents, but not tidal currents, were present. Comparisons were made of wave height, wave set-up and wave-induced longshore currents with good agreement.

7) Comparisons have been made with field measurements of tidal current velocities during calm wave conditions. Good agreement between the model and measurements was obtained. The performance of the model during combined wave and tidal action needs to be investigated, for which a thorough and suitably located field measurement exercise is required.

9 ACKNOWLEDGEMENTS

The author would like to thank his colleague R L Soulsby for his many helpful discussions in the course of this work. Prof B A O'Connor and Dr D Yoo of Liverpool University are thanked for discussions on their wave-current friction model.

10 REFERENCES

1 ABERNETHY C L and GILBERT G. "Refraction of wave spectra", Report IT 117, Hydraulics Research Station, May 1975.

2 BATTJES J A. "Set-up due to irregular waves", Proc. 13th International Conference on Coastal Engineering, ASCE, pp 1993-2004, 1972.

3 BATTJES J A and JANSSEN J P F M. "Energy loss and set-up due to breaking of random waves", Proc 16th International Conference on Coastal Engineering, ASCE, Hamburg, pp569-587, 1978.

4 BIJKER E W. "The increase of bed shear in a current due to wave motion", Proc. 10th International Conference on Coastal Engineering, ASCE, Vol 1, pp 746-765, 1966.

5 BONNETON M and GAILLARD P. "Numerical calculation of wave-induced currents", IAHR 21st Congress, Melbourne, Australia, Aug 1985.

6 BOOIJ N. "Gravity waves on water with non-uniform depth and current", Report No 81-1, Department of Civil Engineering, Delft University of Technology, 1981.

7 BOOIJ N, HOLTHUIJSEN L H and HERBERS T H C. "A numerical model for wave boundary conditions in port design", International Conference on Numerical and Hydraulic Modelling of Ports and Harbours, Birmingham, England, April 1985.

8 BRAMPTON A H and MOTYKA J M. "Recent examples of mathematical models of UK beaches", ASCE Speciality Conference on Coastal Sediments, New Orleans, USA, May 1987.

9 DALRYMPLE R A, KIRBY J T and HWANG P A. "Wave diffraction due to areas of energy dissipation", Journal of Waterway, Port Coastal and Ocean Engineering, ASCE, Vol 110, No 1, Feb 1984.

10 JONSSON I G and CHRISTOFFERSEN J. "Current depth refraction of regular waves", 17th International Conference on Coastal Engineering, ASCE, Houston, U.S.A, 1984.

11 KAMPHUIS J W. "Friction factor under oscillating waves", Journal of Waterways, Harbours and Coastal Engineering Division, ASCE, Vol 101, pp 135-144, 1975.

12 KOMAR P D and INMAN D L. "Longshore sand transport on beaches", Journalof Geophysical Research, Vol 75, No 30, pp 5914-5927, 1970.

13 LE MEHAUTE B and SOLDATE M. "Mathematical modelling of shoreline evolution", CERC Misc. Report No 77-10, 1977.

14 LONGUET-HIGGINS M S. "Longshore currents generated by obliquely incident sea waves 1", Journal of Geophysical Research, Vol 75, No 33, Nov 1970.

15 LONGUET-HIGGINS M S, and STEWART R W, "Radiation stress in water waves; a physical discussion with applications", Deep-Sea Research, Vol 11, pp 529-562, 1964.

16 MICHE M, "Movements Ondulatoires de la mer en profondeur constant ou decroissante", Annales des Ponts et Chaussees, 1944.

17 O'CONNOR B A and YOO D, "Mean bed friction of combined wave-current flow", Coastal Engineering, Vol 12, No 1, March 1988.

18 OZASA H and BRAMPTON A H, "Mathematical modelling of beaches backed by seawalls", Coastal Engineering, Vol 4, No 1, July 1980.

19 PECHON P, "Modelling of longshore currents with a non-linear wave theory", ASCE Speciality Conference on Coastal Hydrodynamics, Delaware, USA 1987.

20 PRICE W A, TOMLINSON K W and WILLIS D H, "Predicting changes in the plan shapes of beaches", 13th International Conference on Coastal Engineering, 1972.

21 Shore Protection Manual. US Army Coastal Engineering Research Centre, US Govt Printing Office. Revised periodically.

22 SKOVGAARD O, JONSSON I G, and BERTELSEN J A, "Computation of wave heights due to refraction and friction", Journal of Waterways, Harbours and Coastal Engineering Division, ASCE, Vol 101, pp 15-32, 1975.

23 SOUTHGATE H N, "Current-depth refraction of water waves. A description and verification of three numerical models", Report SR 14, Hydraulics Research Ltd, Jan 1985.

24 SOUTHGATE H N. "A one-dimensional model of wave-current interaction", ASCE Speciality Conference on Coastal Hydrodynamics, Delaware, USA, 1987.

25 SOUTHGATE H N. "Wave breaking. A review of techniques for calculating energy losses in breaking waves", Report SR 168, Hydraulics Research Ltd, March 1988.

26 STIVE M J F, and DE VRIEND H J. "Quasi-3D nearshore current modelling: wave-induced secondary current", ASCE Speciality Conference on Coastal Hydrodynamics, Delaware, USA, 1987.

27 SVENDSEN I A. "Wave heights and set-up in a surf zone", Coastal Engineering, Vol 8, pp 303-329, 1984.

28 SWART D H. "Offshore sediment transport and equilibrium beach profiles", Delft Hydraulics Laboratory. Pub no 131, 1974.

29 THORNTON E B and GUZA R T. "Surfzone longshore currents and random waves: field data and models", Journal of Physical Oceanography, Vol 16, No 7, pp1165-1178, 1986.

30 TOWNEND I M and SAVELL I A. "The application of ray methods to wave refraction studies", Offshore amd Coastal Modelling, 7th POLYMODEL Conference, Sunderland Polytechnic, 1984.

31 TRELOAR P D. "Spectral wave refraction under the influence of depth and current", Coastal Engineering, Vol 9, pp439-452, 1986.

32 VISSER P J. "The proper longshore current in a wave basin", Report No 82-1, Department of Civil Engineering, Delft University of Technology, 1982.

33 VISSER P J. "A mathematical model of the uniform longshore currents and the comparison with laboratory data", Report No 84-2, Department of Civil Engineering, Delft University of Technology, 1984a.

34 VISSER P J. "Uniform longshore current measurements and calculations", 19th International Conference on Coastal Engineering, ASCE, Houston, USA, 1984b.

35 WEGGEL J R. "Maximum breaker height", Journal of Waterways, Harbours and Coastal Engineering Division, ASCE, Vol 98, 1972.

36 WIND H G and VREUGDENHIL C B. "Rip-current generation near structures", Journal of Fluid Mechanics, Vol 171, pp459-476, 1986.

37 YOO D. "Mathematical modelling of wave-current interacted flow in shallow waters", PhD thesis, University of Manchester, 1986.

38 YOO D and O'CONNOR B A. "Mathematical modelling of wave-induced nearshore circulations", 20th International Conference on Coastal Engineering, ASCE, Taipei, Taiwan, 1986.

39 YOO D and O'CONNOR B A ."Bed friction model of wave-current interacted flow", ASCE Speciality Conference on Coastal Hydrodynamics, Delaware, USA, 1987.

11 LIST OF SYMBOLS

a	Breaking parameter Eq 4.7.4.
a'	Empirical breaking factor
A_o	Semi-excursion length of water particle at seabed
b	Breaking parameter Eq 4.7.5.
C_{fc}	Current friction factor with wave interaction
C'_{fc}	Current friction factor without wave interaction
C_{fw}	Wave friction factor with current interaction
C'_{fw}	Wave friction factor without current interaction
c_{ga}	Absolute wave group velocity Eq 4.4.5.
c_{gr}	Relative wave group velocity Eq 4.4.4.
c_r	Relative wave celerity Eq 4.4.3.
D_b	Spatial rate of dissipation of wave energy flux due to breaking
D_f	Spatial rate of dissipation of wave energy flux due to seabed friction
E	Wave energy per unit sea area. Eq 4.5.2.
$f(q)$	Defined by Eq 5.6.11
$f(q)_{min}$	Minimum value of f(q). Eq 5.6.14.
$f(Q)$	Defined by Eq 4.7.12
F	Driving force from wave radiation stresses Eq 4.9.8
g	Acceleration due to gravity
G	Defined by Eq 5.6.8
h	Water depth
H	Wave height
H_b	Wave height at the breaker point
H_n	Root-mean-square wave height in the Rayleigh distribution assuming no truncation
H_{rms}	Root-mean-square wave height in the Rayleigh distribution with truncation
i	$\sqrt{-1}$
k	Wavenumber
k_s	Seabed roughness length

K_d	Doppler coefficient Eq 4.8.8
K_r	Refraction coefficient Eq 4.8.7
K_s	Shoaling coefficient Eq 4.8.6
m	Seabed slope
P(H)	Rayleigh probability distribution of wave heights Eq 4.7.1
q	Defined by Eq 5.6.9
q_{min}	Value of q corresponding to minimum value of f(q) Eq 5.6.15
Q	Probability of occurrence of a broken wave Eq 4.7.8
S	Surface slope due to longshore tidal variations
S_m	Maximum value of oscillatory component of S
S_o	Steady component of S
S_{xy}	Wave radiation stress in the longshore direction
S_{yy}	Wave radiation stress in the onshore direction
t	Time
U	Longshore current velocity
U_m	Maximum value of tidal-oscillatory component of U
U_o	Steady component of U
V_o	Maximum water particle velocity at seabed
x	Longshore coordinate
y	Onshore coordinate
α	Angle between wave orthogonal and onshore direction
β	Wave energy dissipation factor Eq 4.8.9
γ	Empirical breaking factor in Miche expression Eq 4.7.2
δ	Angle between longshore current and onshore direction
ε	Wave energy dissipation factor Eq 4.9.7
ζ	Surface elevation above mean sea level
ζ_m	Maximum value of ζ
η	Wave set-up

θ	Phase of oscillatory component of S
λ	Empirical breaking factor
μ	Angle between wave ray and onshore direction Eq 4.4.6
ρ	Water density
τ	Shear stress at the seabed
τ_{td}	Time-dependent component of τ
τ_{ti}	Time-independent component of τ
ϕ	Phase of ζ
ψ	Phase of tidal-oscillatory component of U
ω	Tidal angular frequency
ω_a	Absolute wave angular frequency
ω_r	Relative wave angular frequency Eq 4.4.2

Subscripts

i	Denotes present grid point
o	Denotes previous grid point (further offshore)
j	Iteration number

Table

Table 1 Beach and Wave values used in Visser's Experiments

Expt No	Beach Type	Beach Slope	Wave Period sec	Incident Values			Values at breaker line			Max Wave setup cm	Breaker Type
				Depth cm	Wave Angle degr	Wave Height cm	Depth cm	Wave Angle degr	Wave Height cm		
1	smooth	0.101	2.01	39.9	31.1	7.2	10.4	20.9	10.5	4.20	plunging
2	smooth	0.101	1.00	39.9	30.5	9.5	10.9	24.0	10.0	2.78	plunging
3	smooth	0.101	1.00	40.1	15.4	8.9	11.4	12.1	9.7	2.75	Plunging
4	smooth	0.050	1.02	35.0	15.4	7.8	11.0	12.5	9.1	1.64	plunging
5	smooth	0.050	1.85	34.8	15.4	7.1	11.6	11.5	10.8	2.45	plunging
6	smooth	0.050	0.70	35.0	15.4	5.9	8.8	14.3	5.8	1.00	spilling/ plunging
7	rough	0.050	1.02	35.0	15.4	7.8	12.2	12.2	9.0	1.64	plunging

Figures

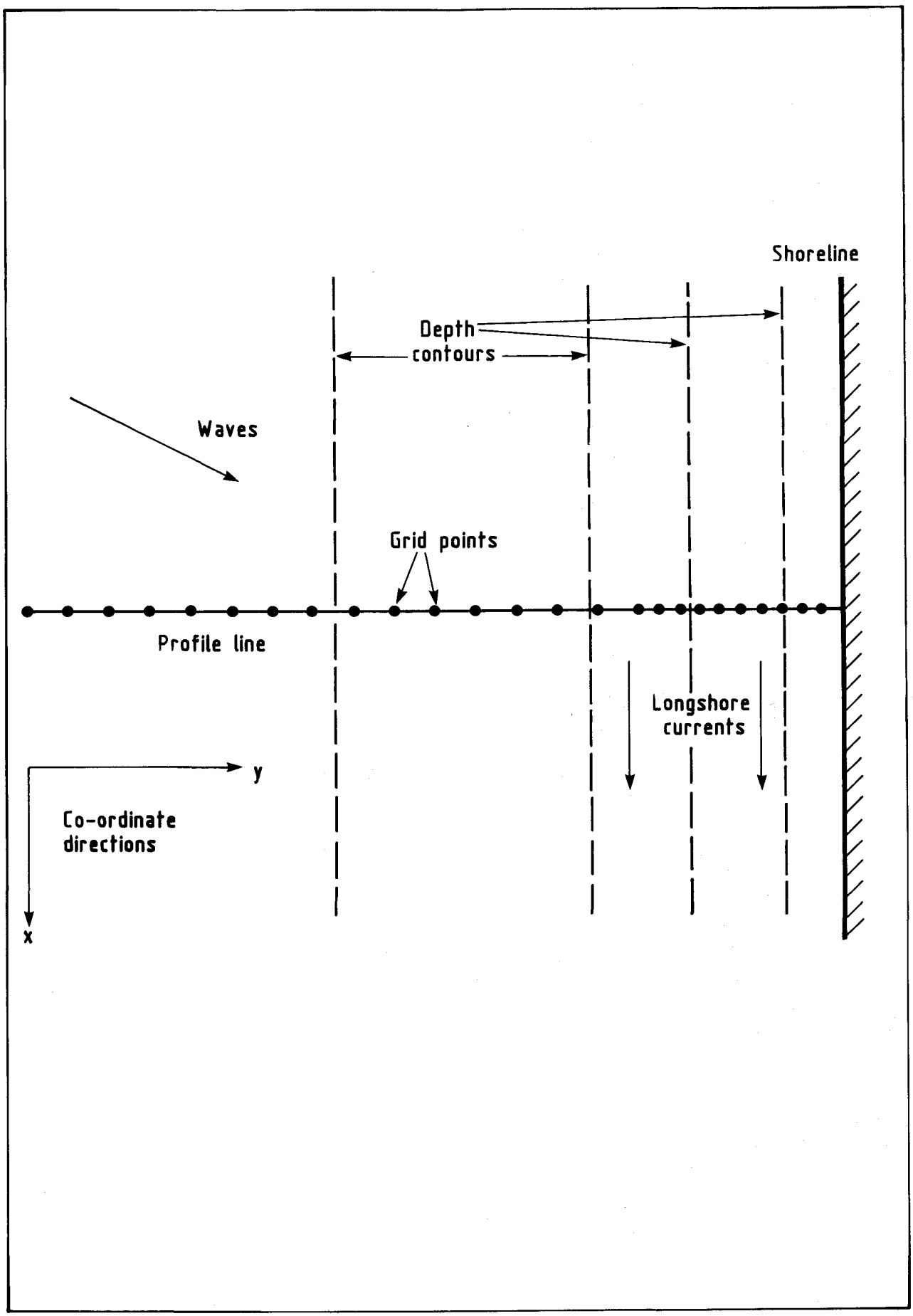

Fig 1 Representation of the nearshore region used in the Nearshore Profile Model

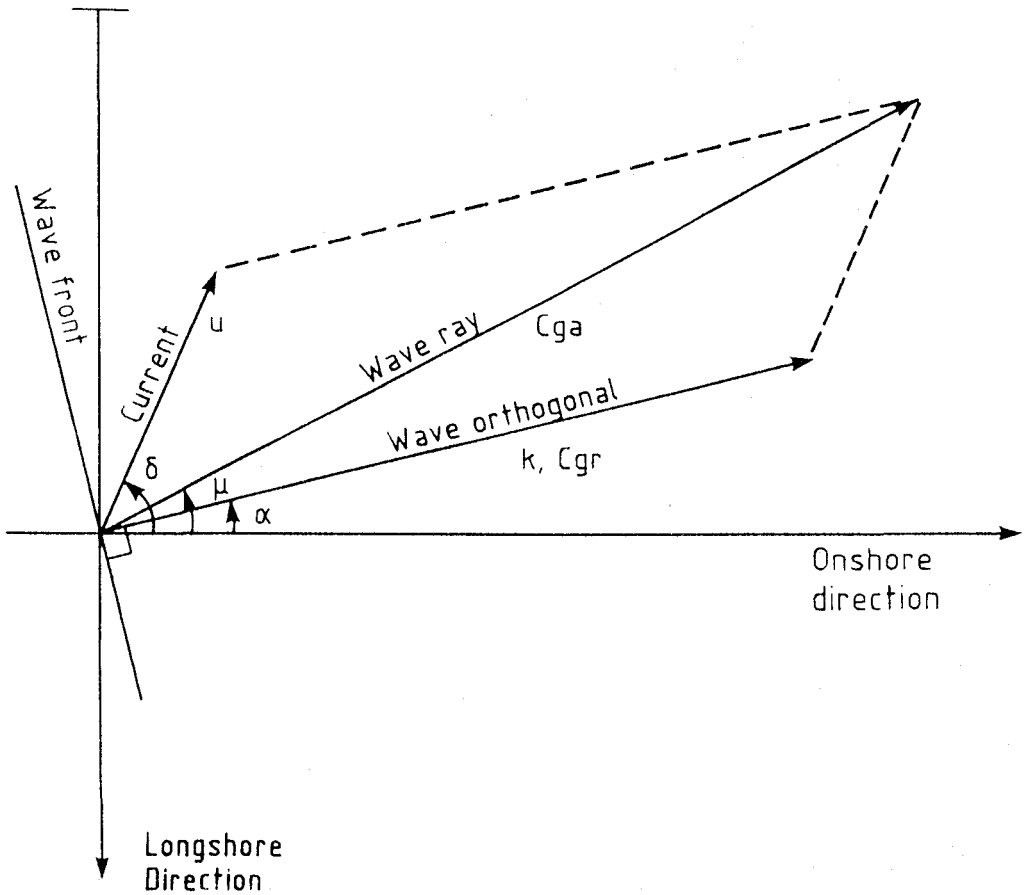

Fig 2 Geometry of currents, wave orthogonals and wave rays

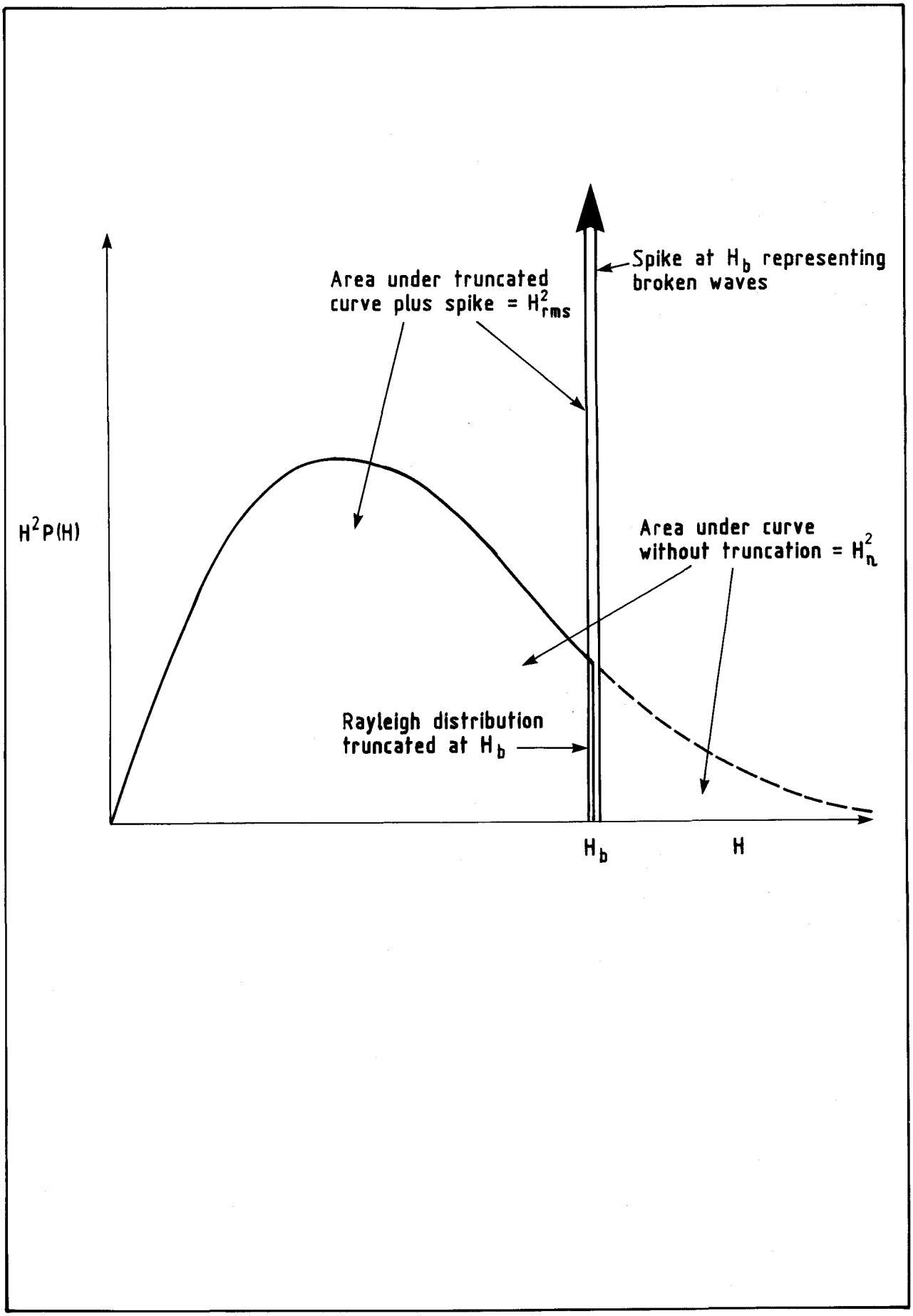

Fig 3 Truncated Rayleigh distribution of wave heights for broken waves

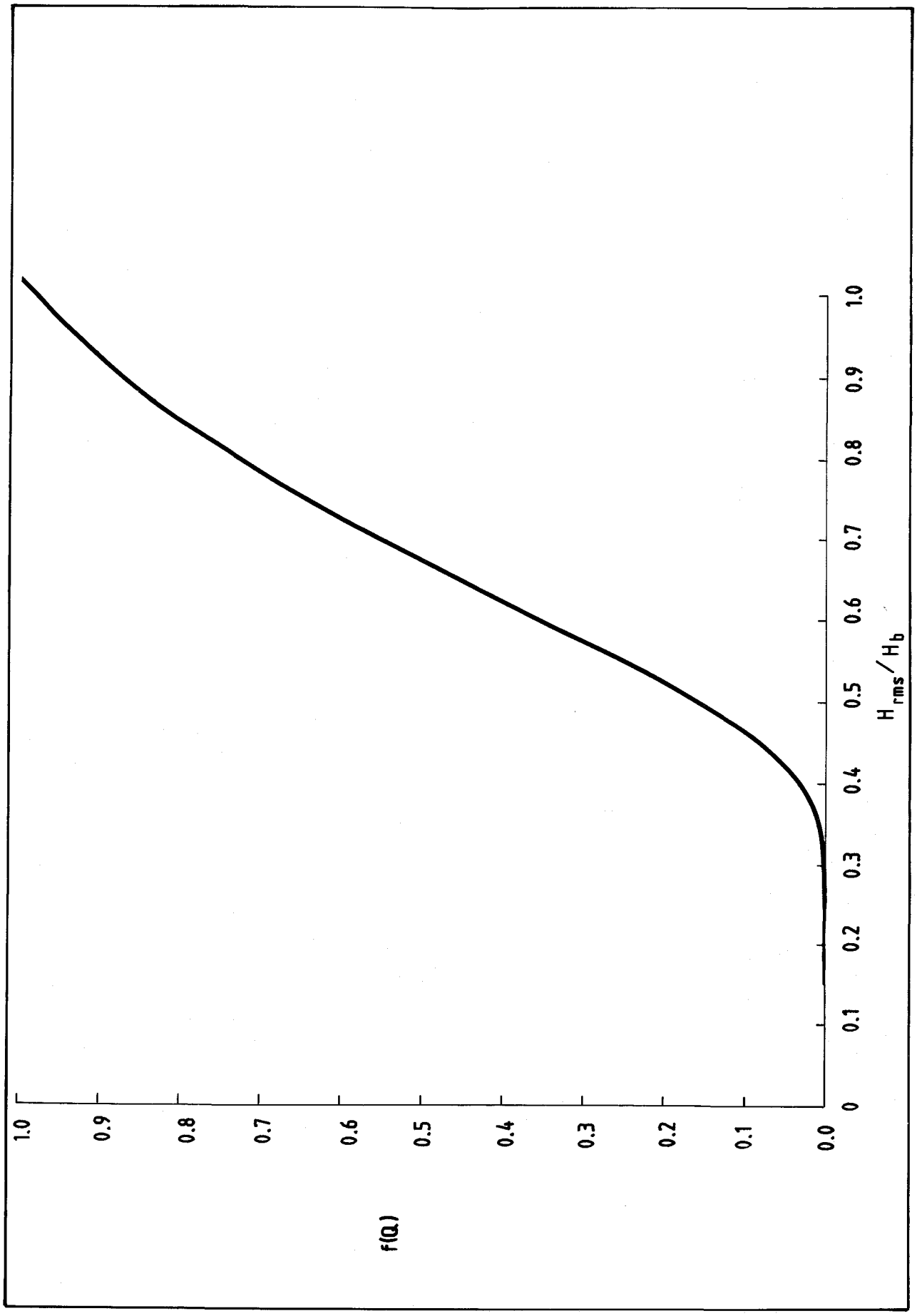

Fig 4 Graph of f(Q) against H_{rms}/H_b (see Equations 4.7.8 and 4.7.12)

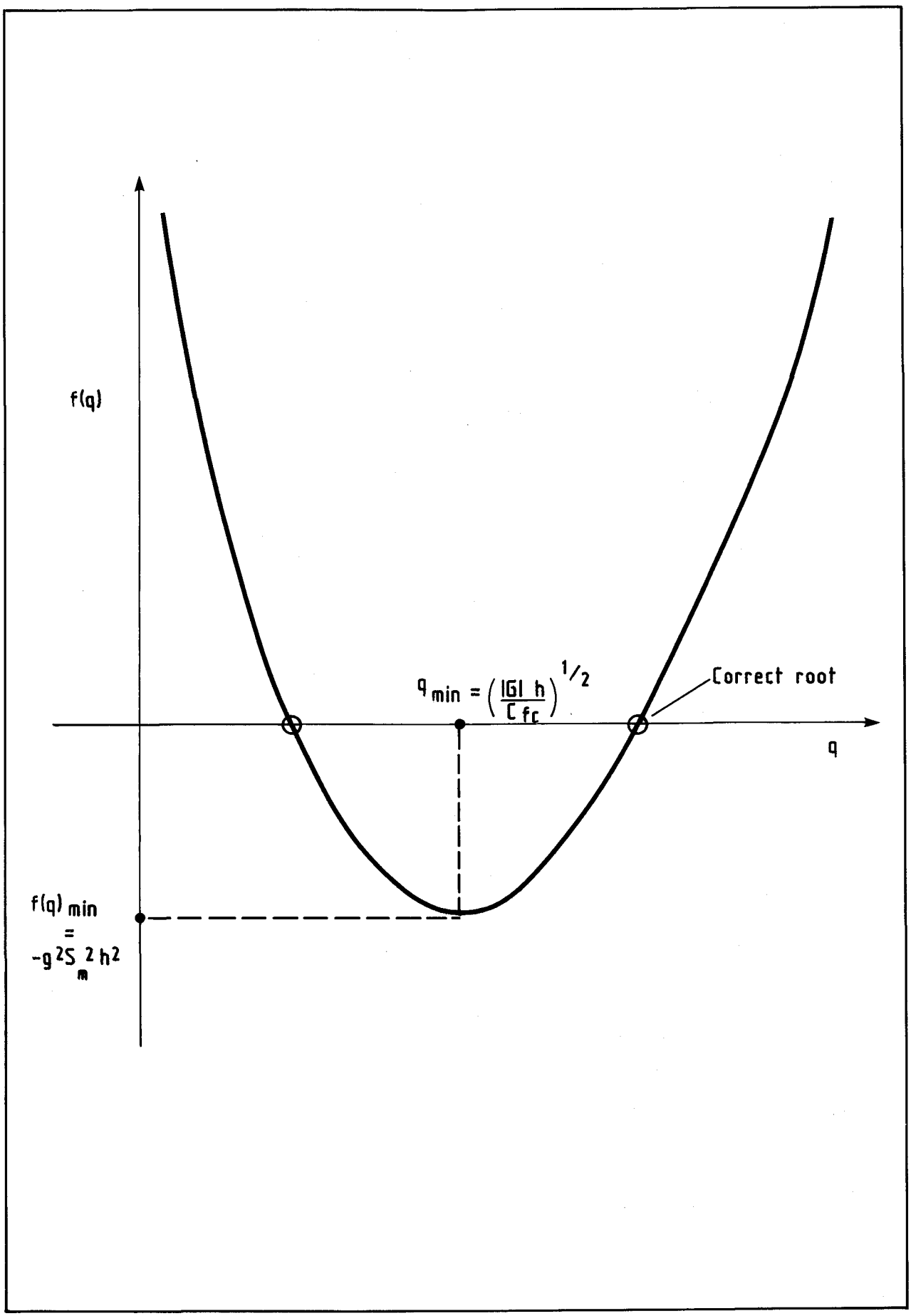

Fig 5 Graph of f(q) (Equation 5.6.11) against q

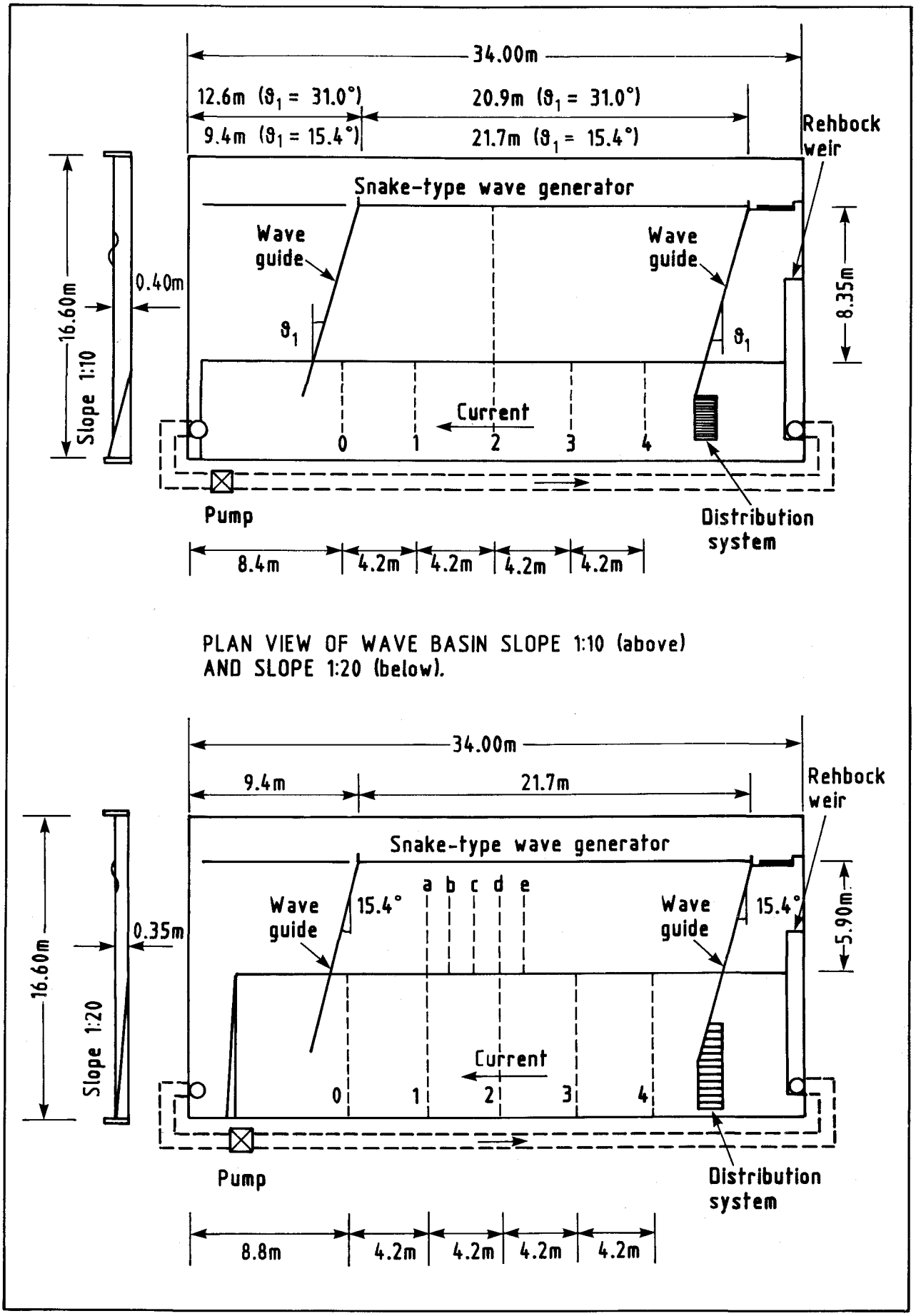

Fig 6 Experimental arrangement used by Visser (from Visser (1984a))

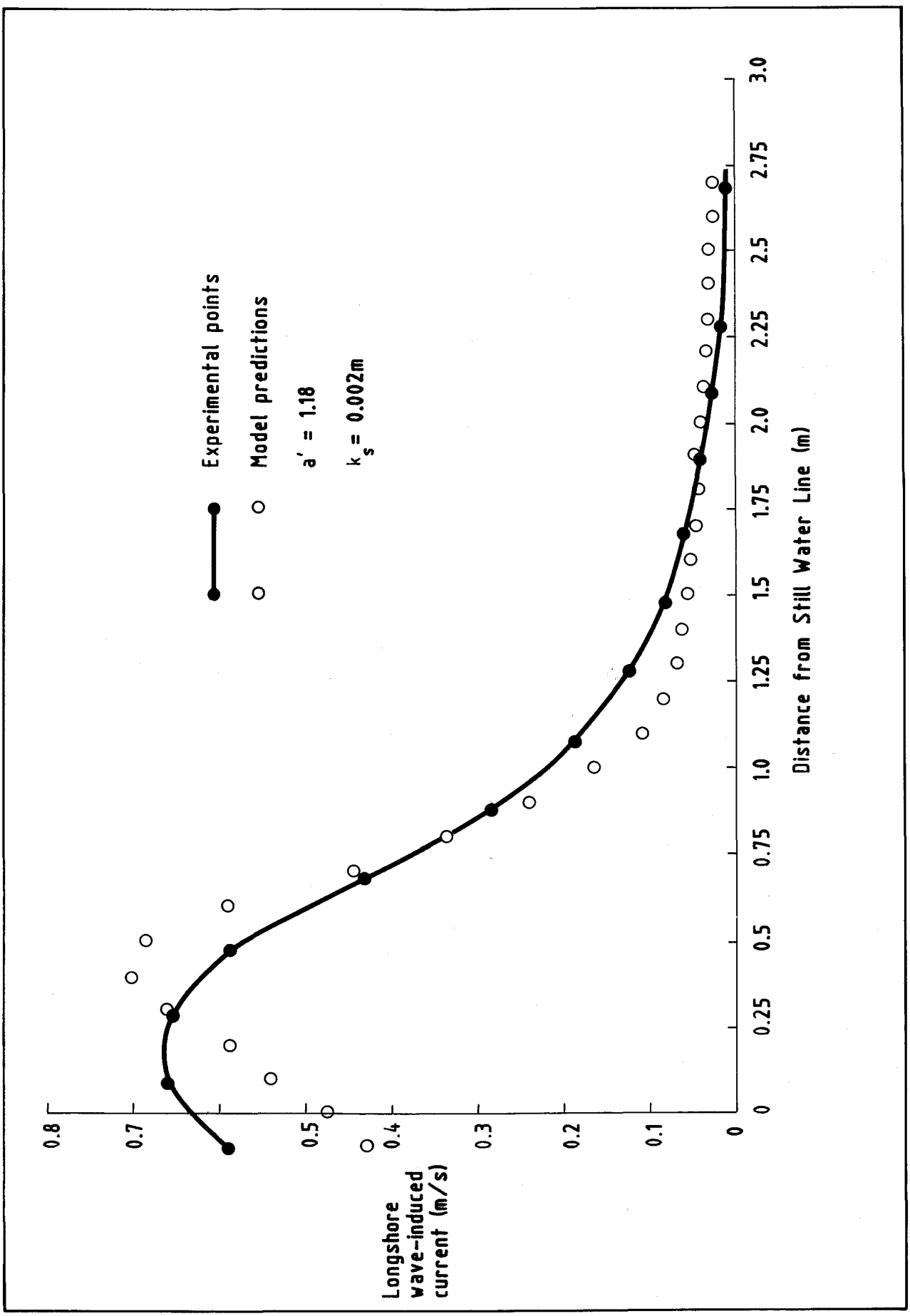

Fig 7 Comparison of Visser Test 1 with Nearshore Profile Model. Longshore currents

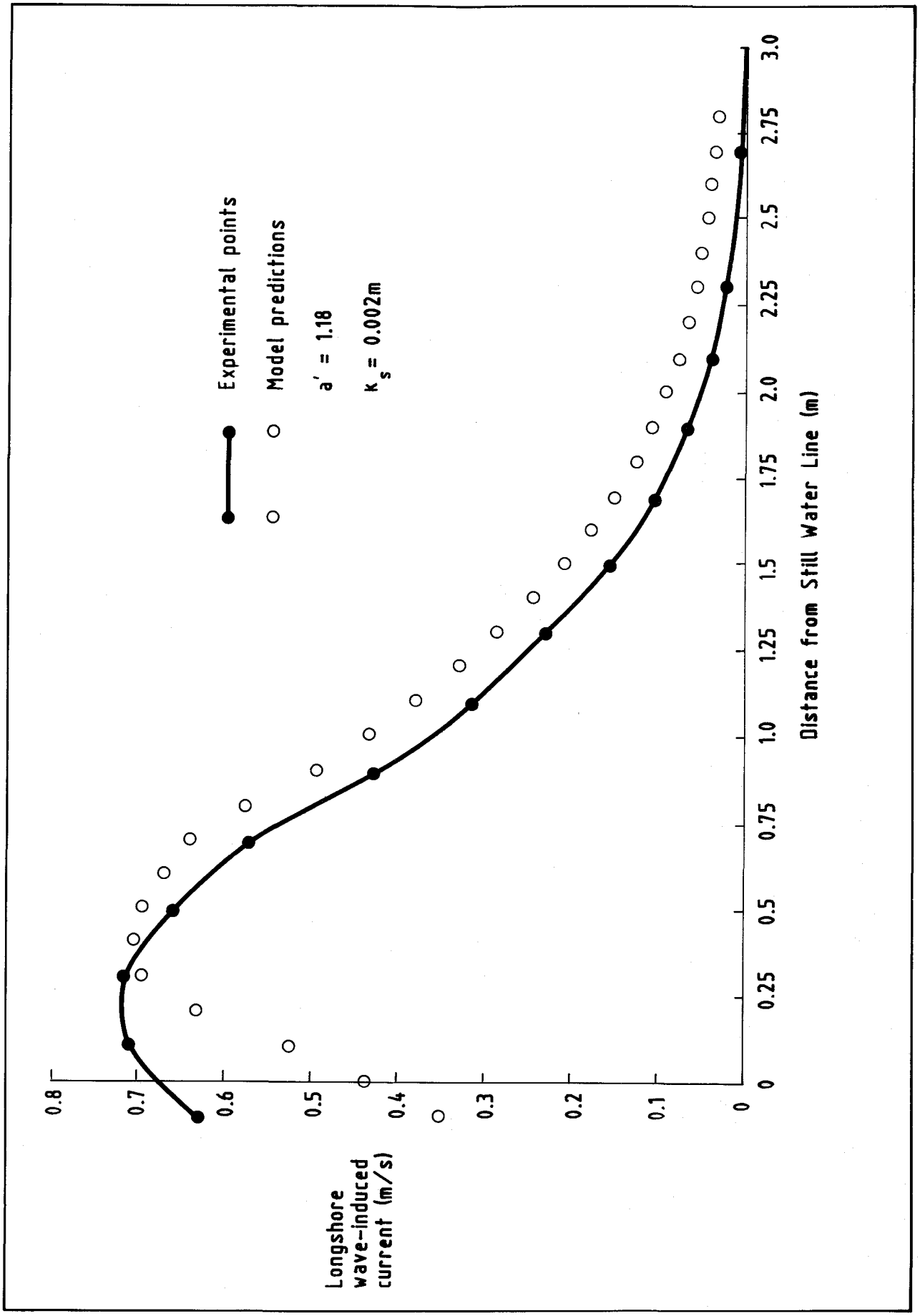

Fig 8 Comparison of Visser Test 2 with Nearshore Profile Model. Longshore currents

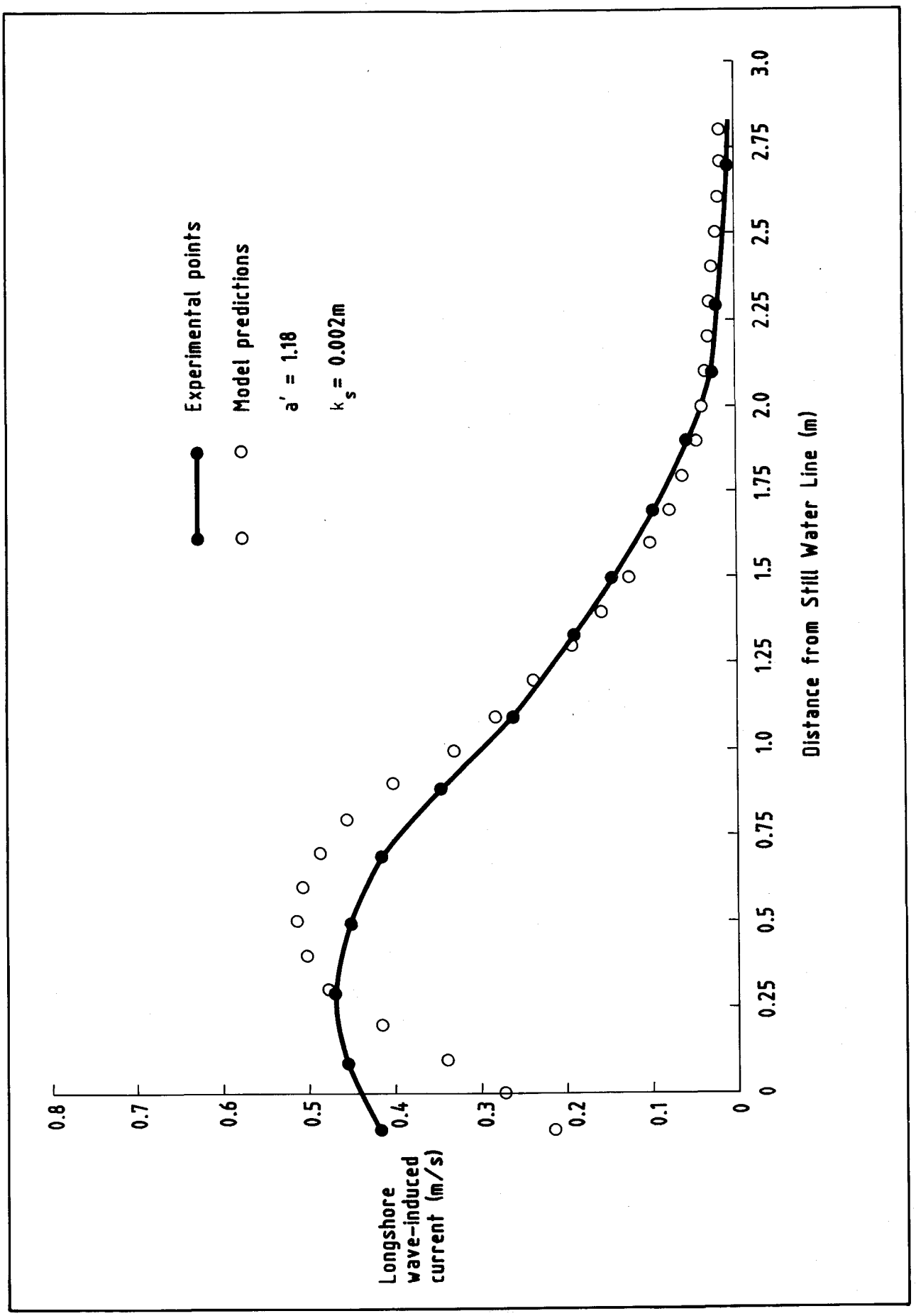

Fig 9 Comparison of Visser Test 3 with Nearshore Profile Model. Longshore currents

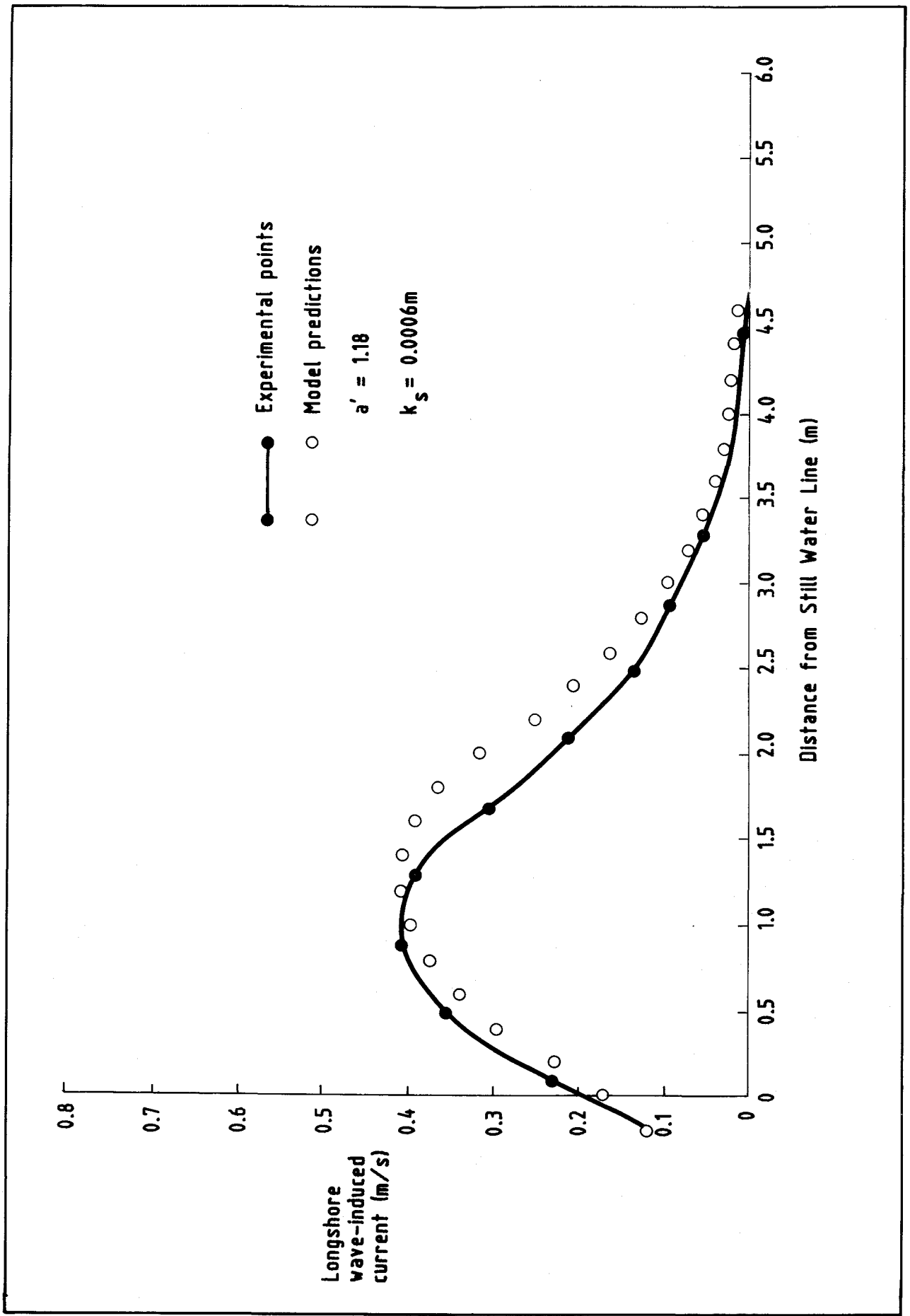

Fig 10 Comparison of Visser Test 4 with Nearshore Profile Model. Longshore currents

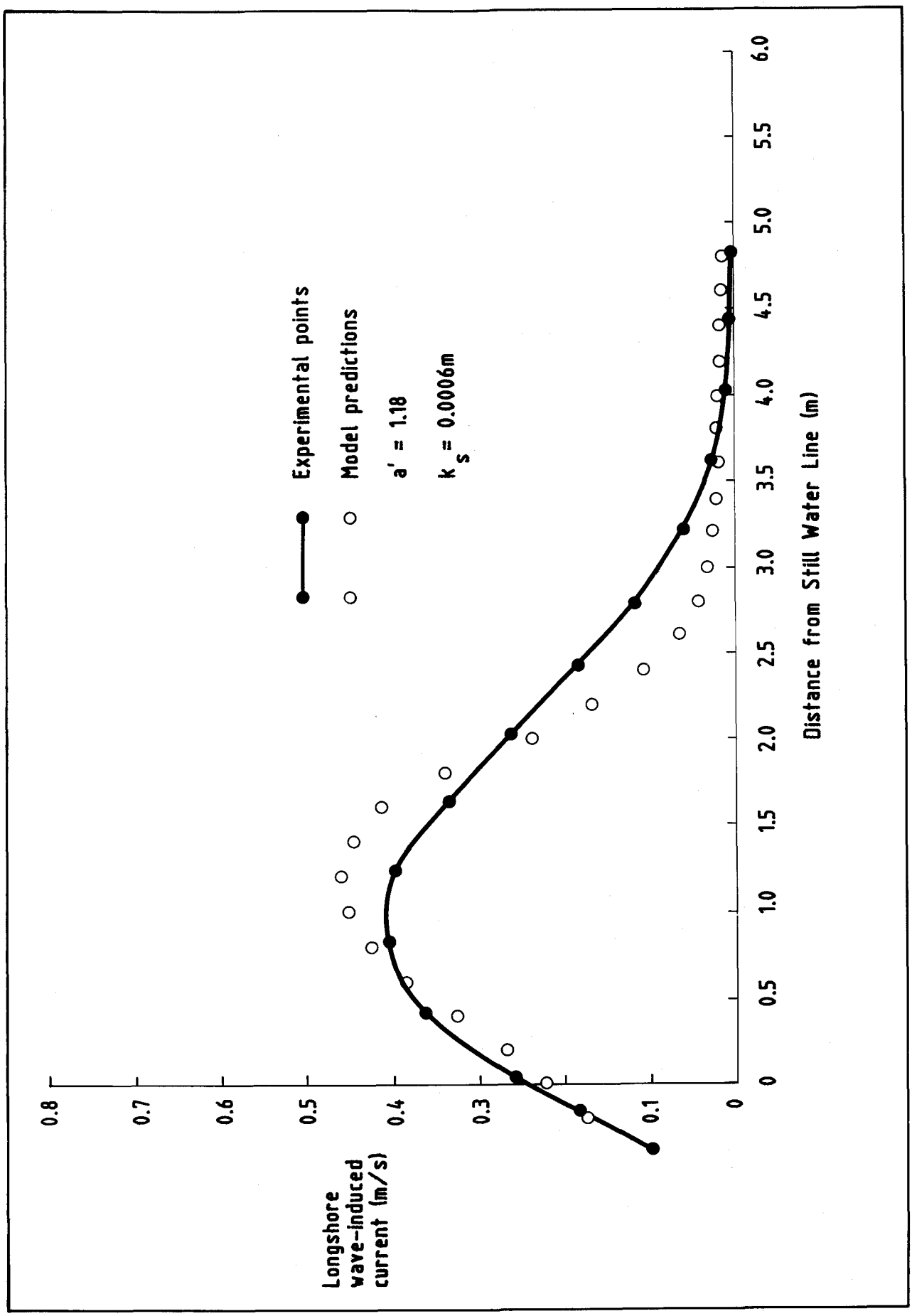

Fig 11 Comparison of Visser Test 5 with Nearshore Profile Model. Longshore currents

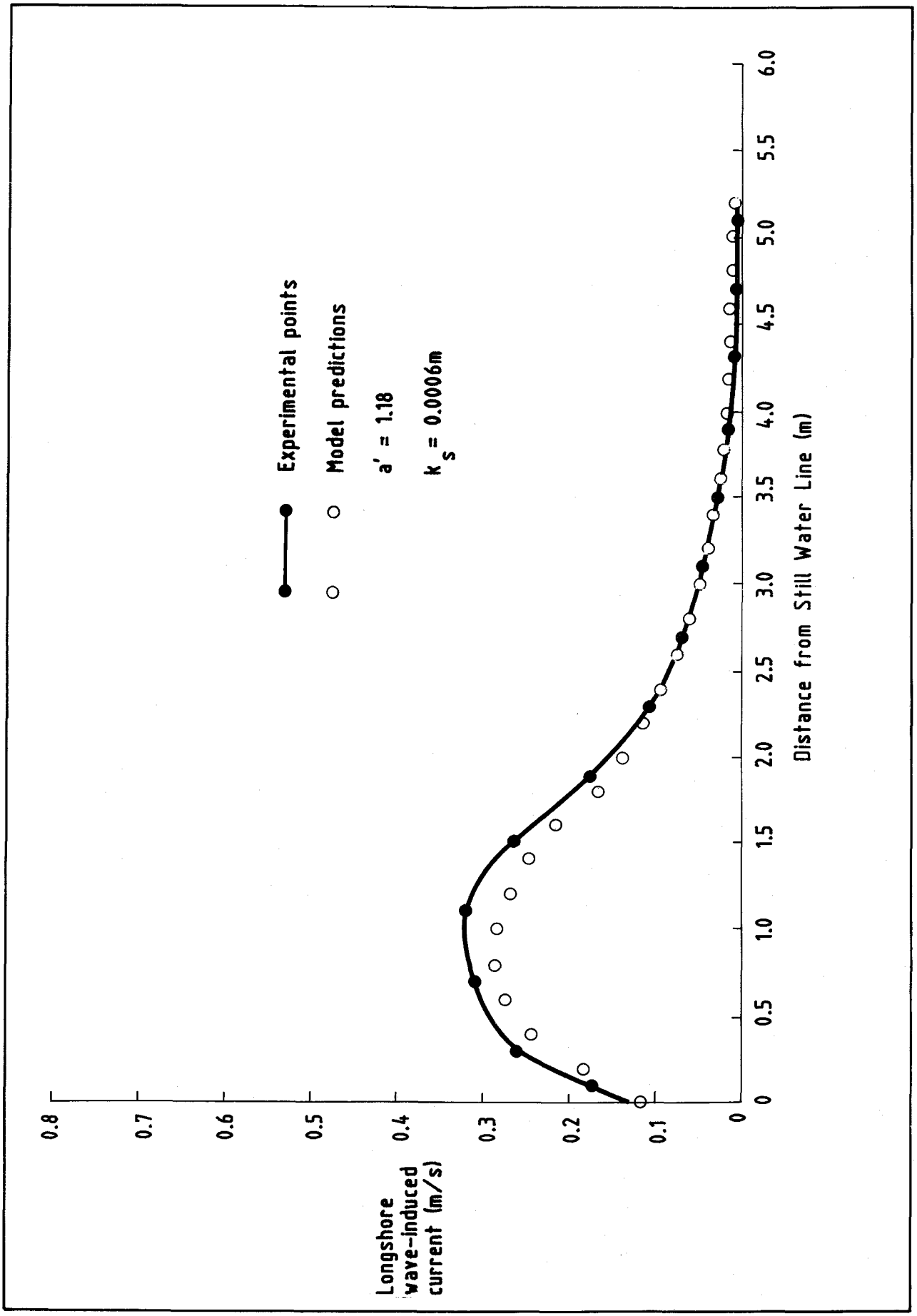

Fig 12 Comparison of Visser Test 6 with Nearshore Profile Model. Longshore currents

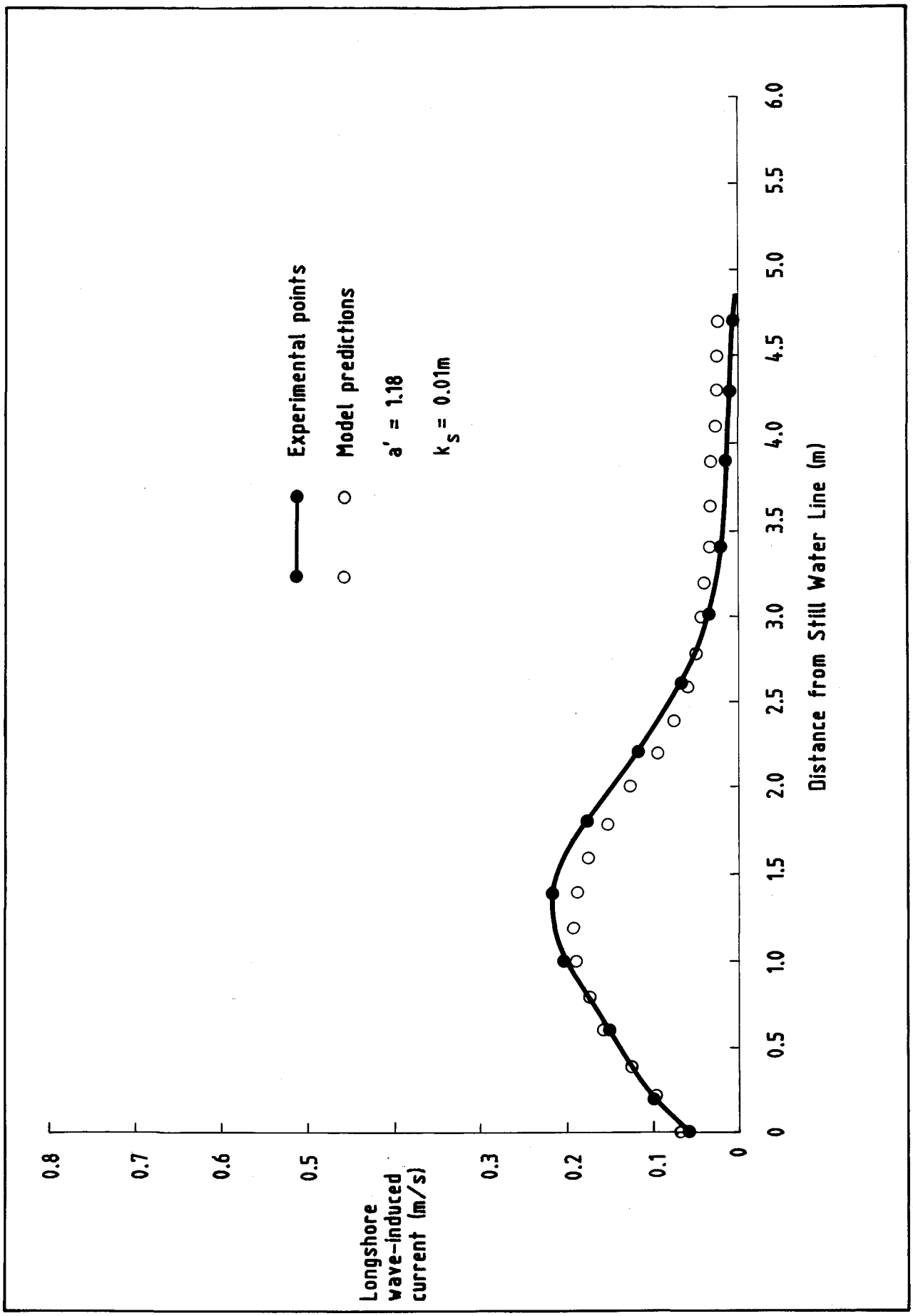

Fig 13 Comparison of Visser Test 7 with Nearshore Profile Model. Longshore currents

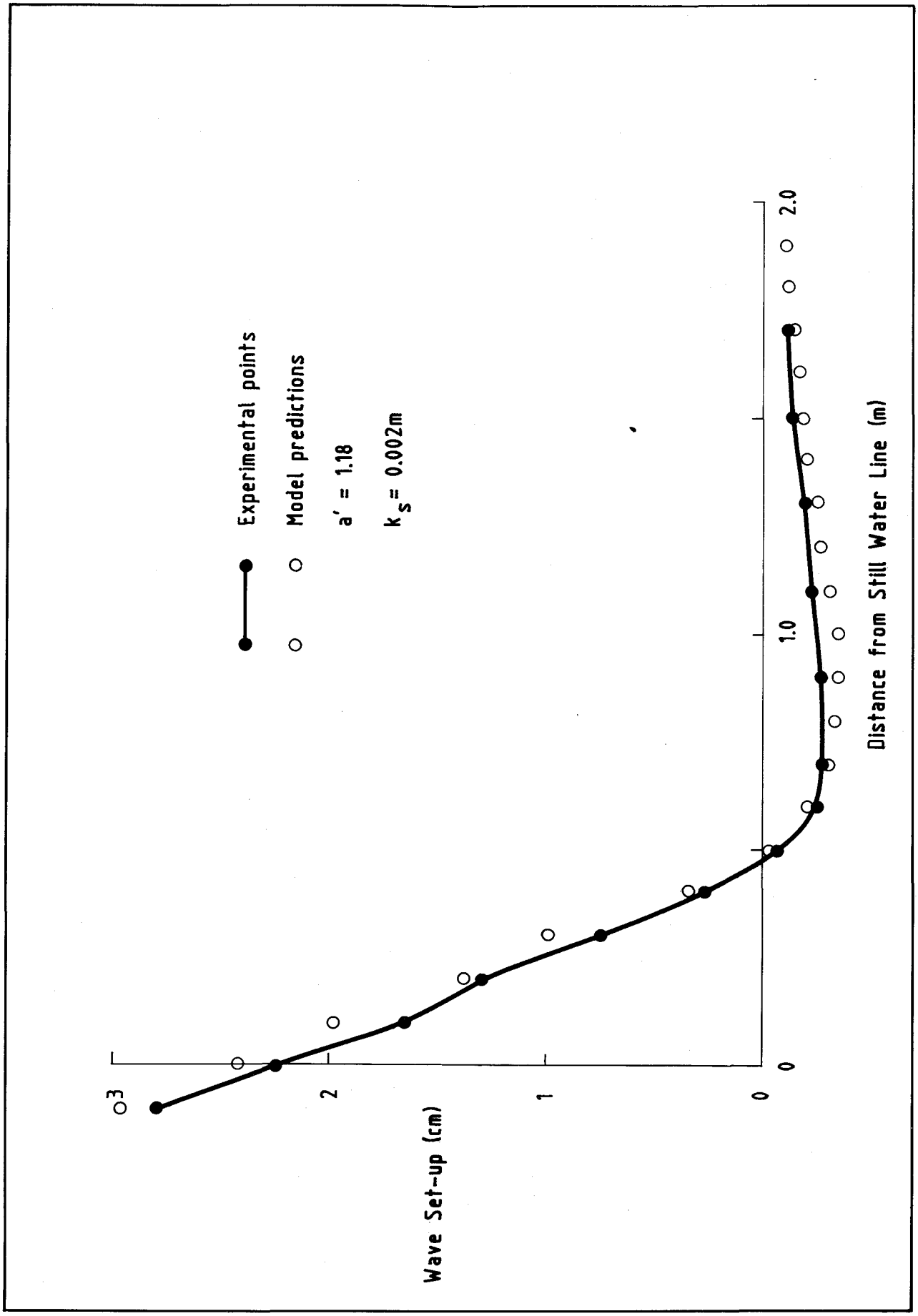

Fig 14 Comparison of Visser Test 1 with Nearshore Profile Model. Wave Set-up

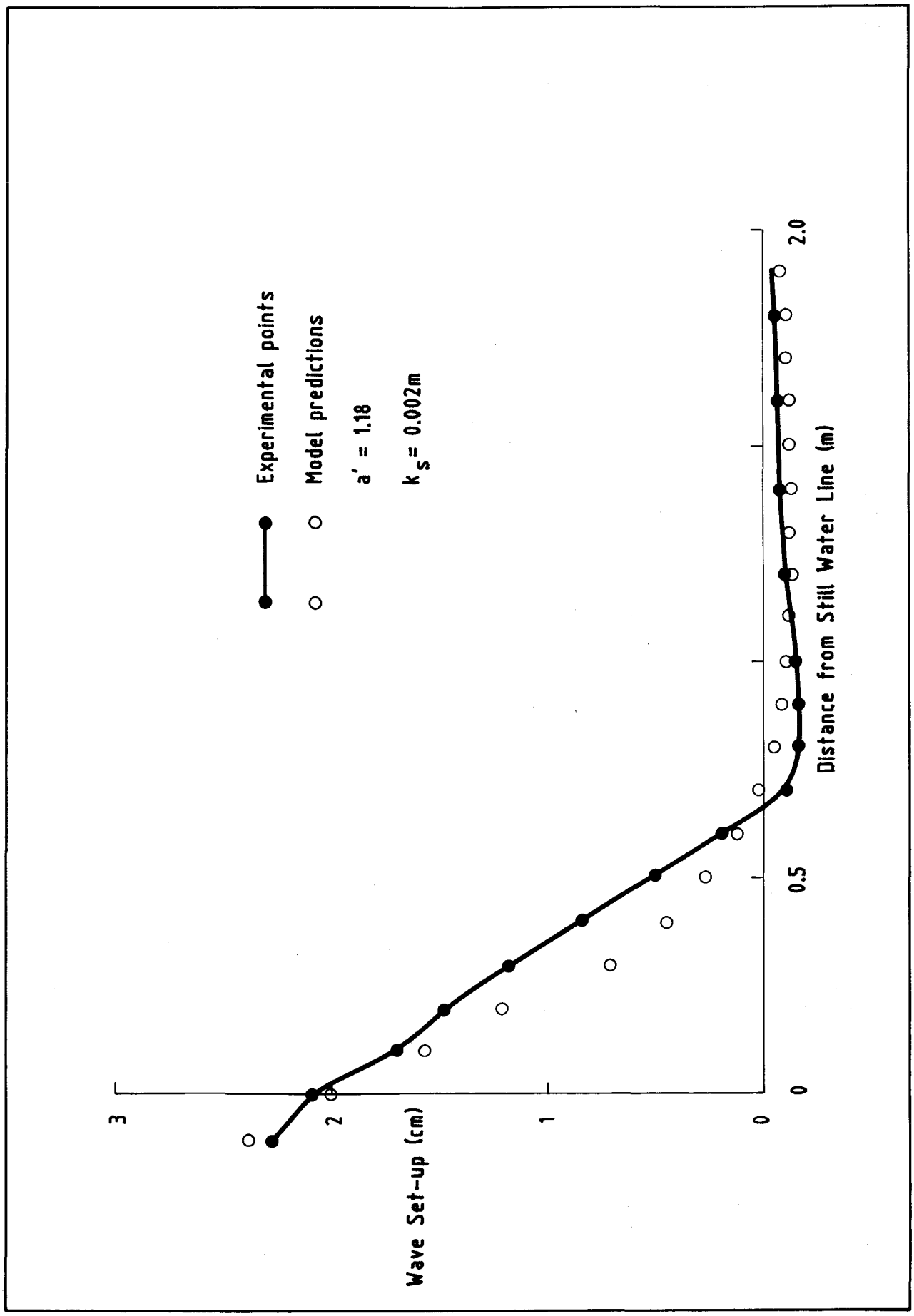

Fig 15 Comparison of Visser Test 2 with Nearshore Profile Model. Wave Set-up

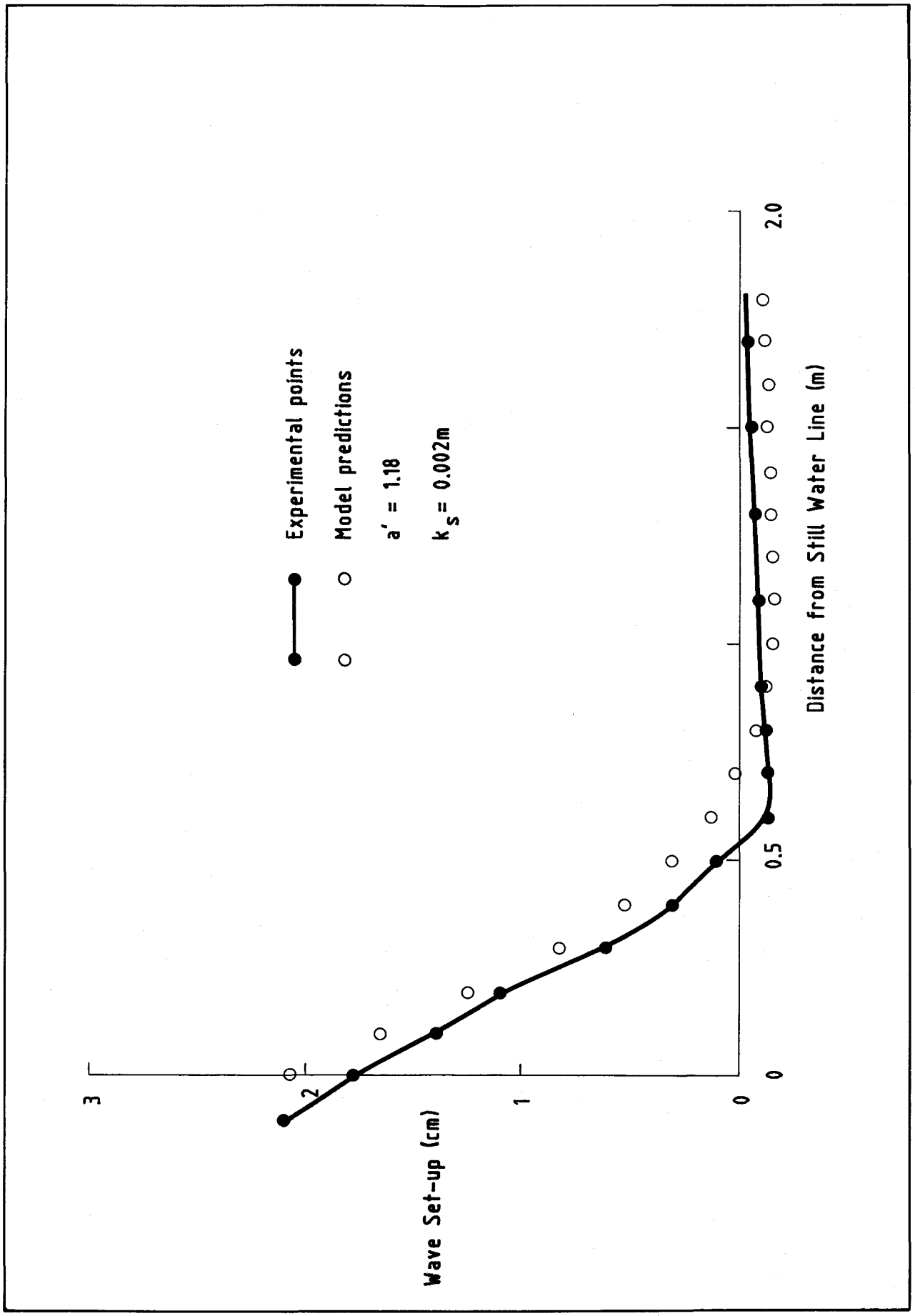

Fig 16 Comparison of Visser Test 3 with Nearshore Profile Model. Wave Set-up

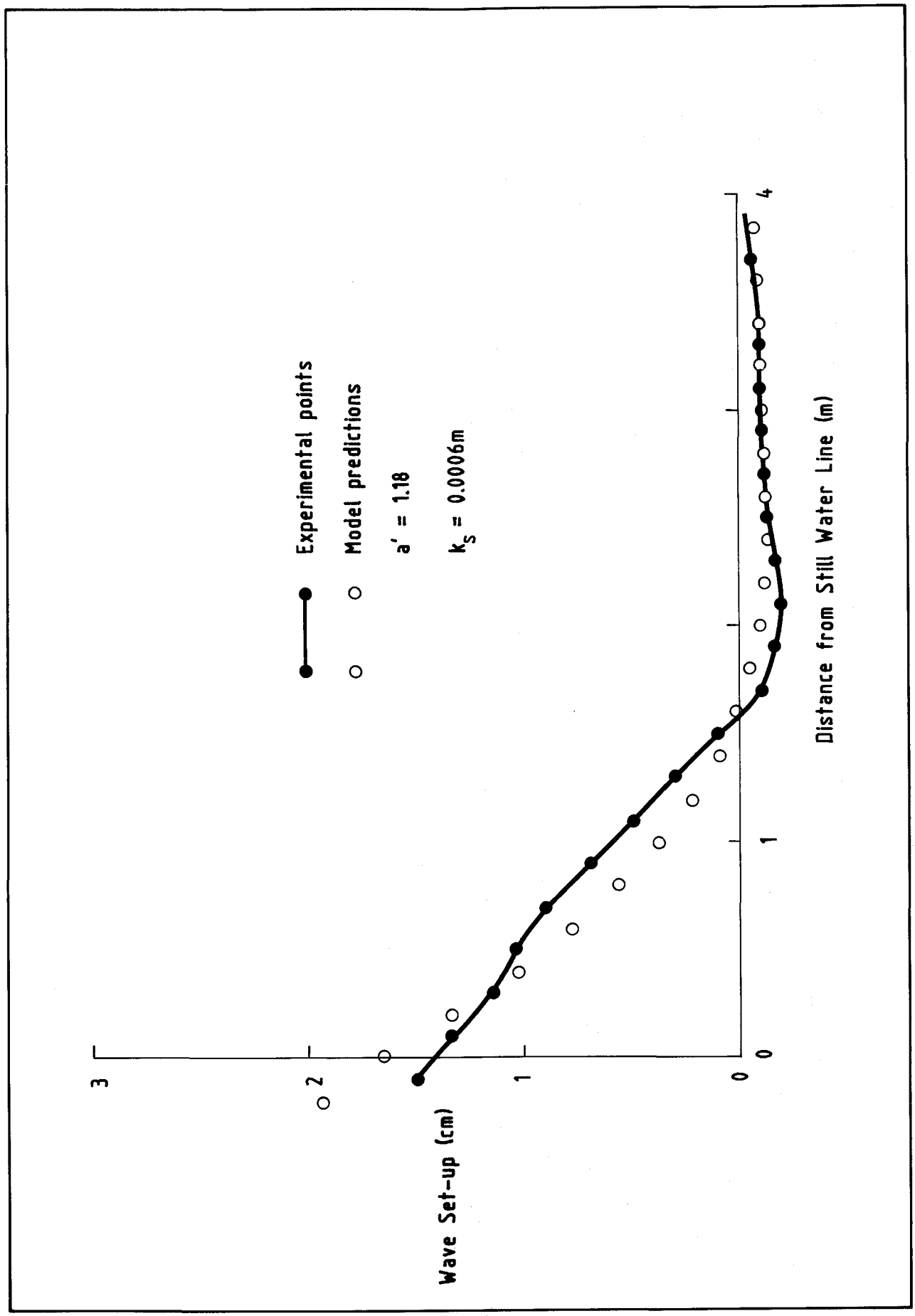

Fig 17 Comparison of Visser Test 4 with Nearshore Profile Model. Wave Set-up

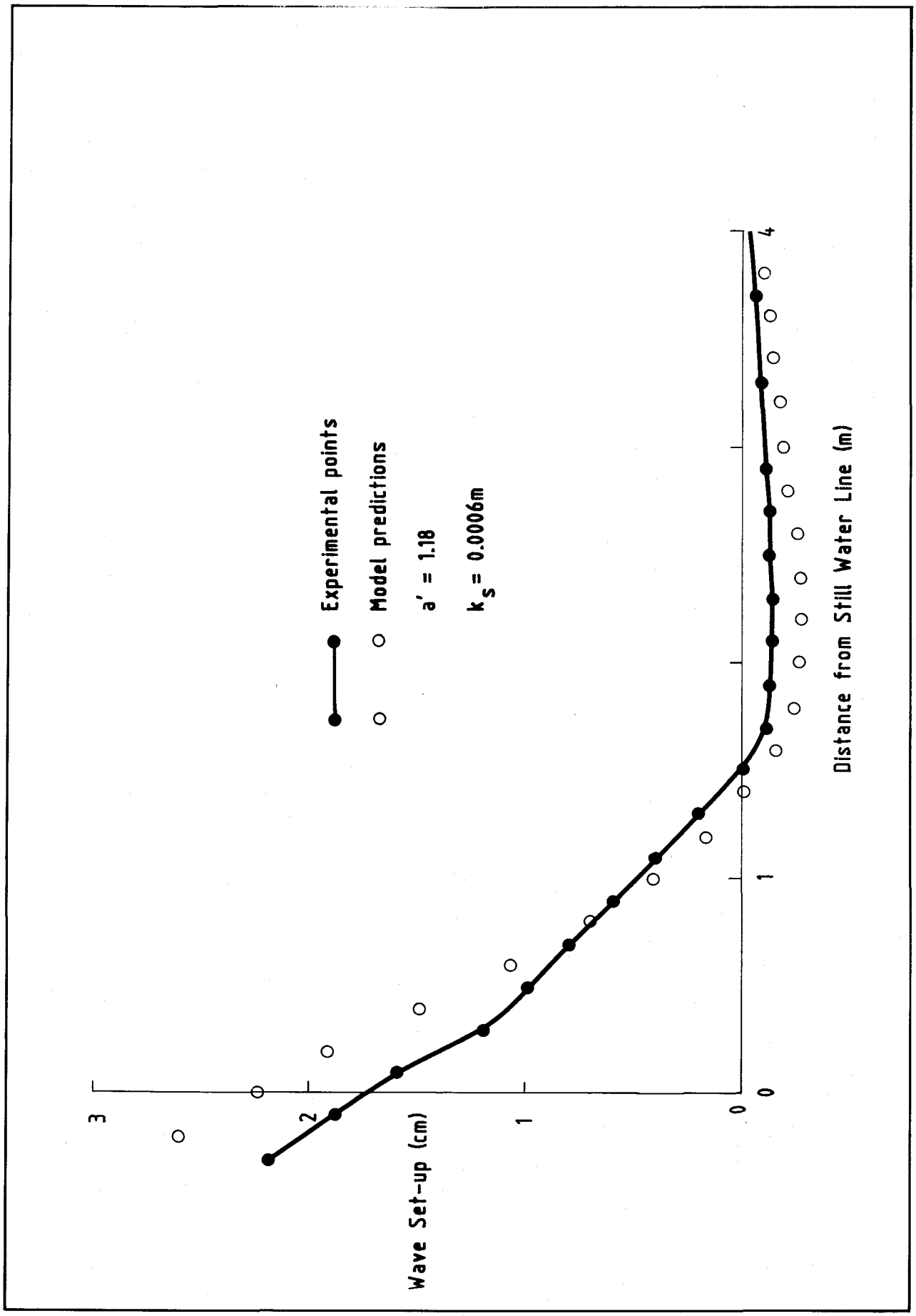

Fig 18 Comparison of Visser Test 5 with Nearshore Profile Model. Wave Set-up

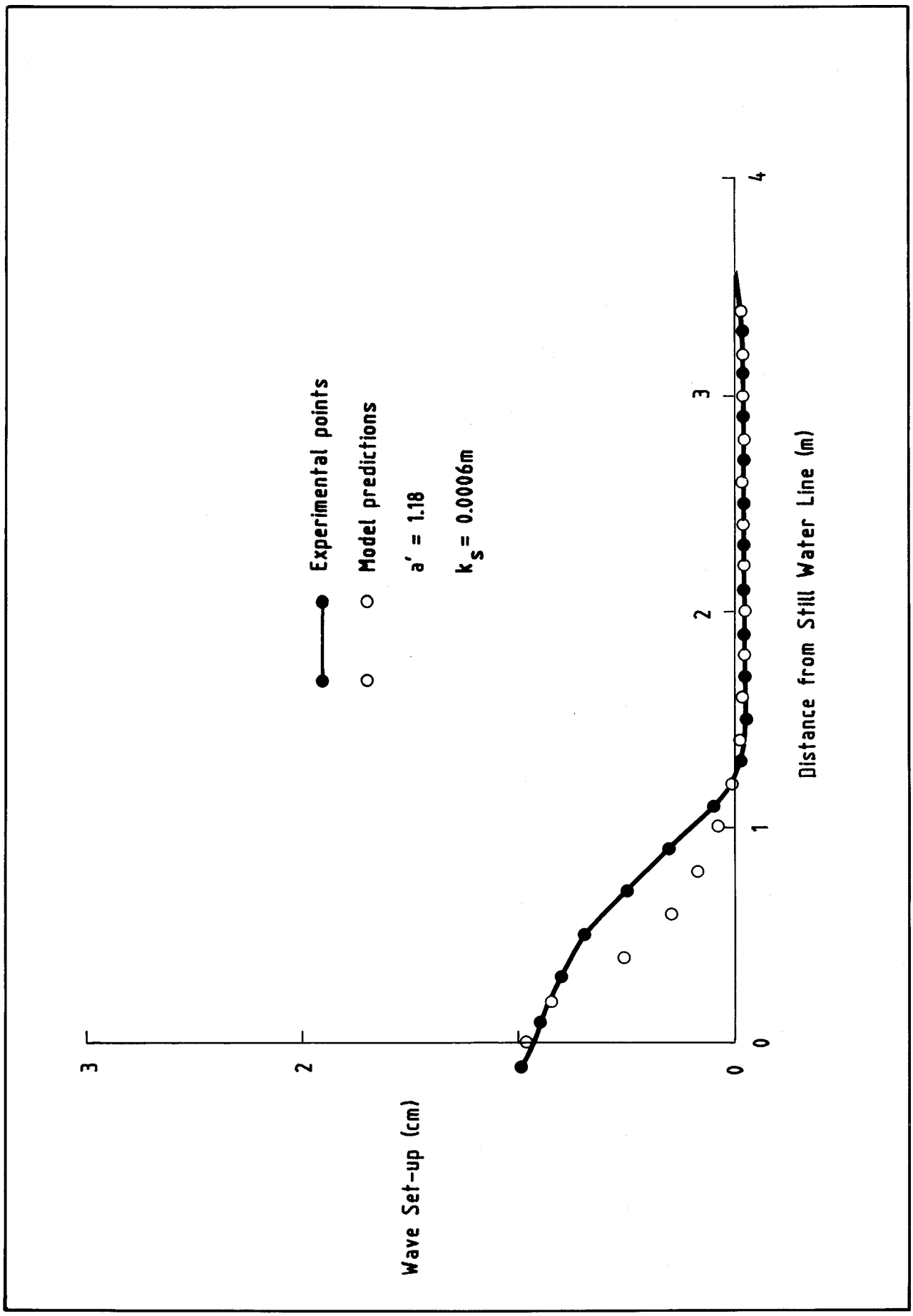

Fig 19 Comparison of Visser Test 6 with Nearshore Profile Model. Wave Set-up

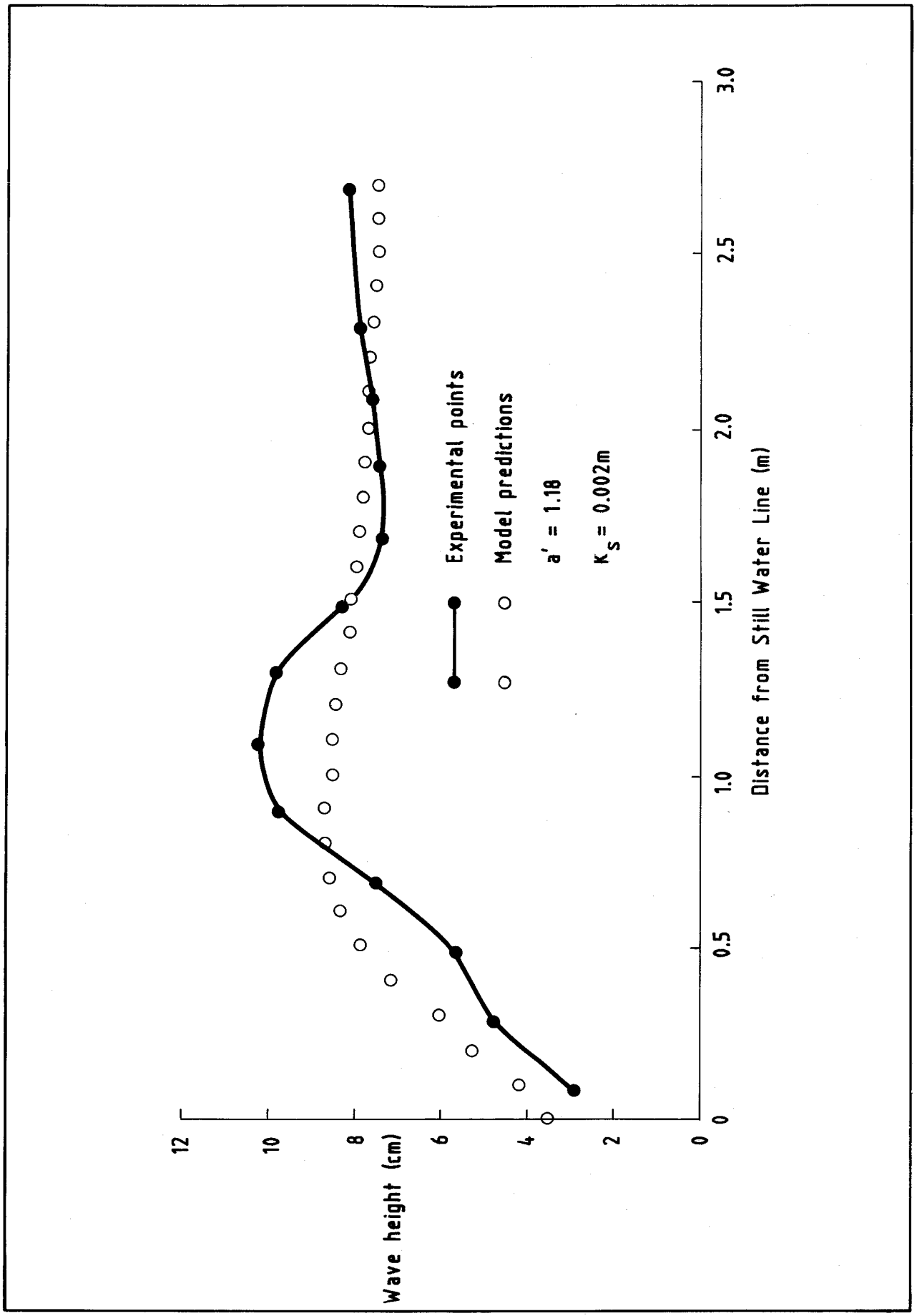

Fig 20 Comparison of Visser Test 1 with Nearshore Profile Model. Wave heights

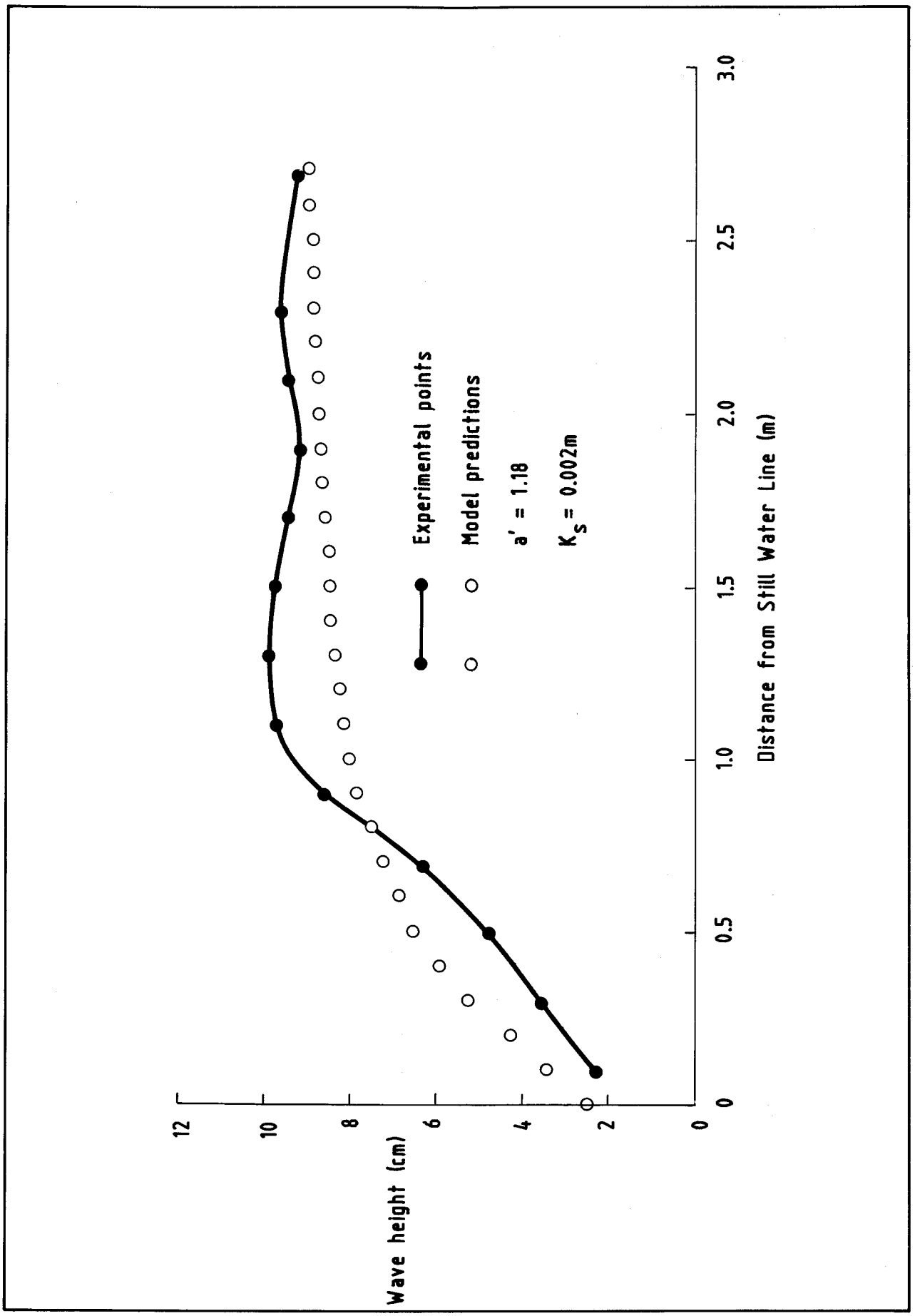

Fig 21 Comparison of Visser Test 2 with Nearshore Profile Model. Wave heights

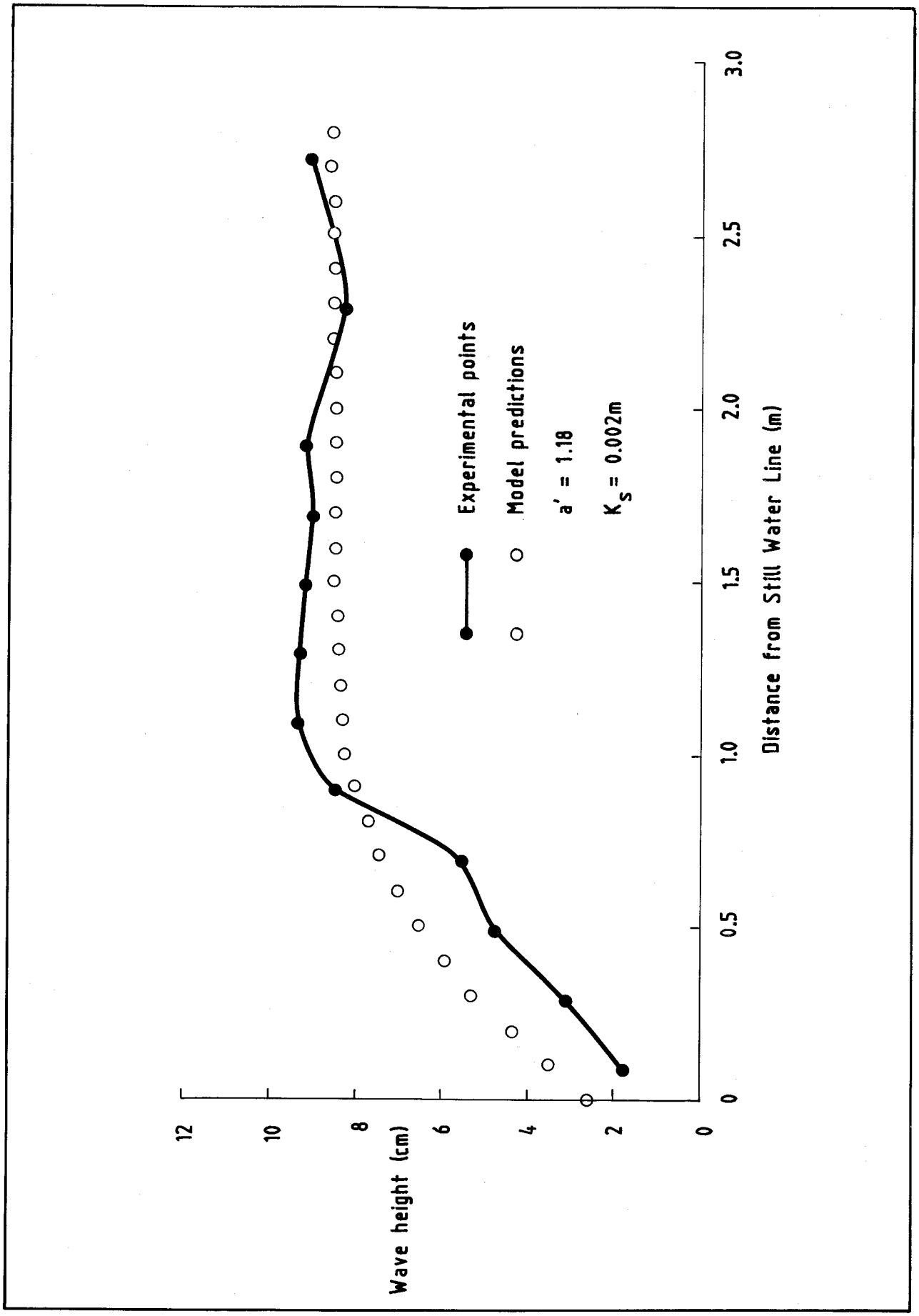

Fig 22 Comparison of Visser Test 3 with Nearshore Profile Model. Wave heights

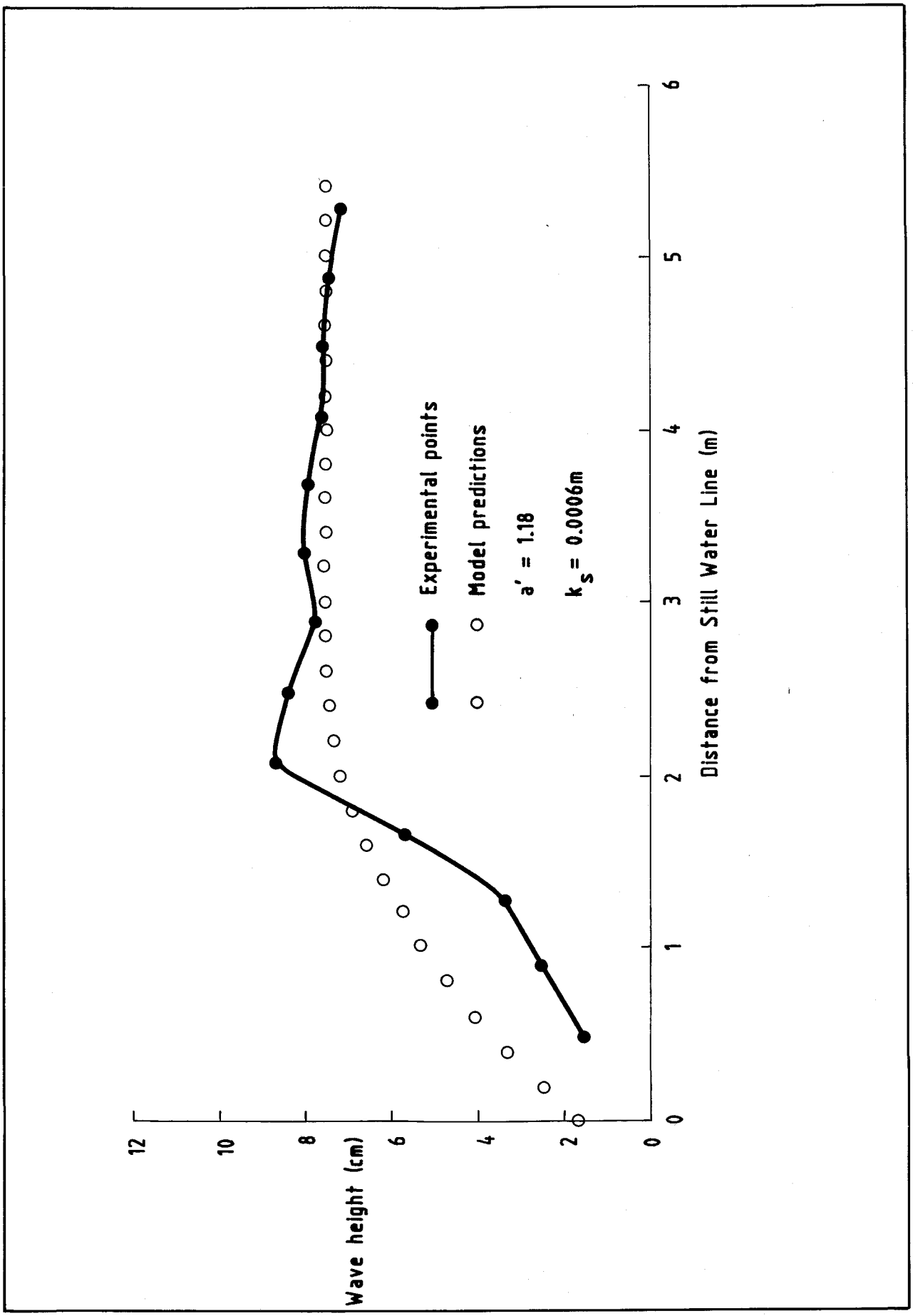

Fig 23 Comparison of Visser Test 4 with Nearshore Profile Model. Wave heights

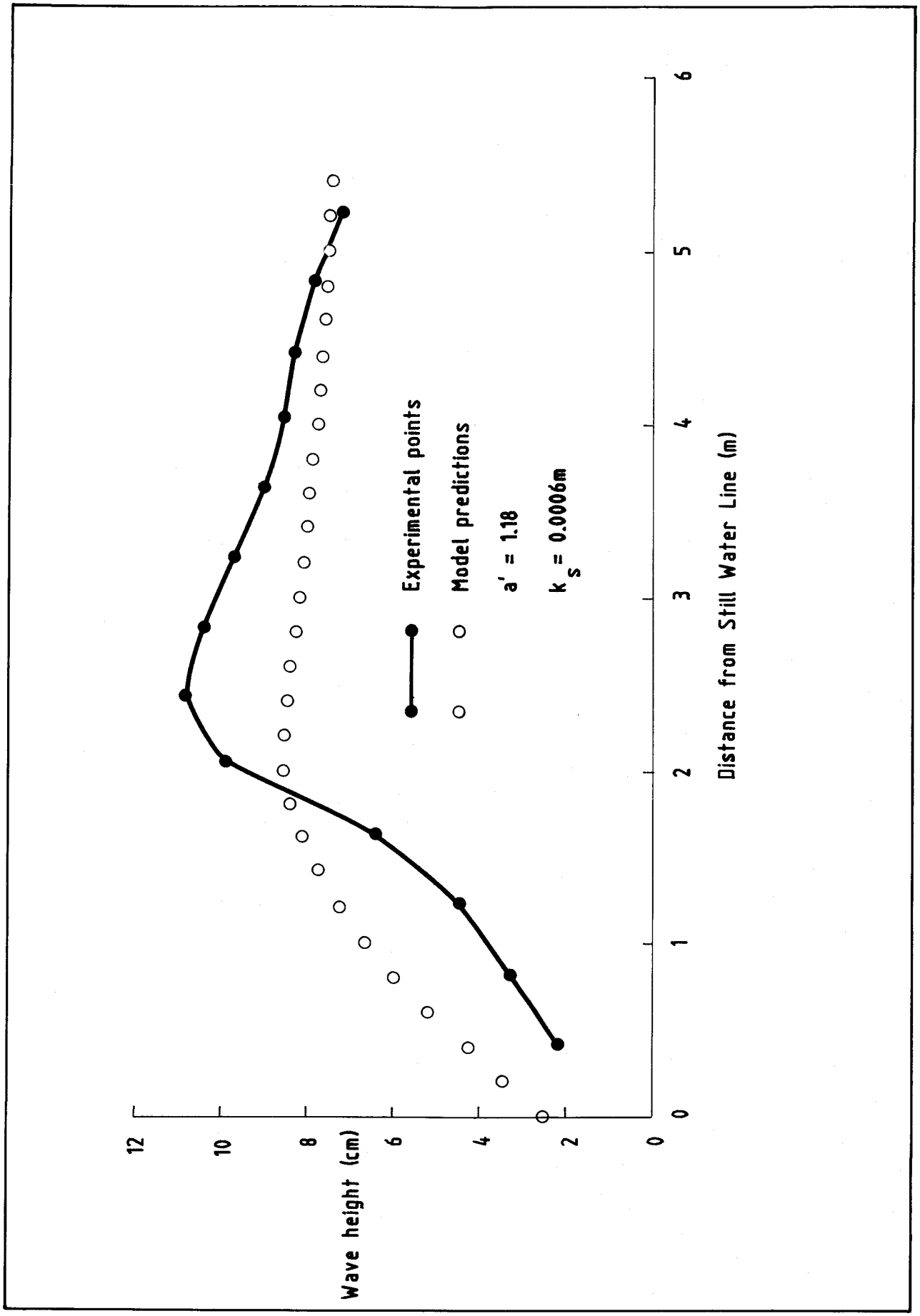

Fig 24 Comparison of Visser Test 5 with Nearshore Profile Model. Wave heights

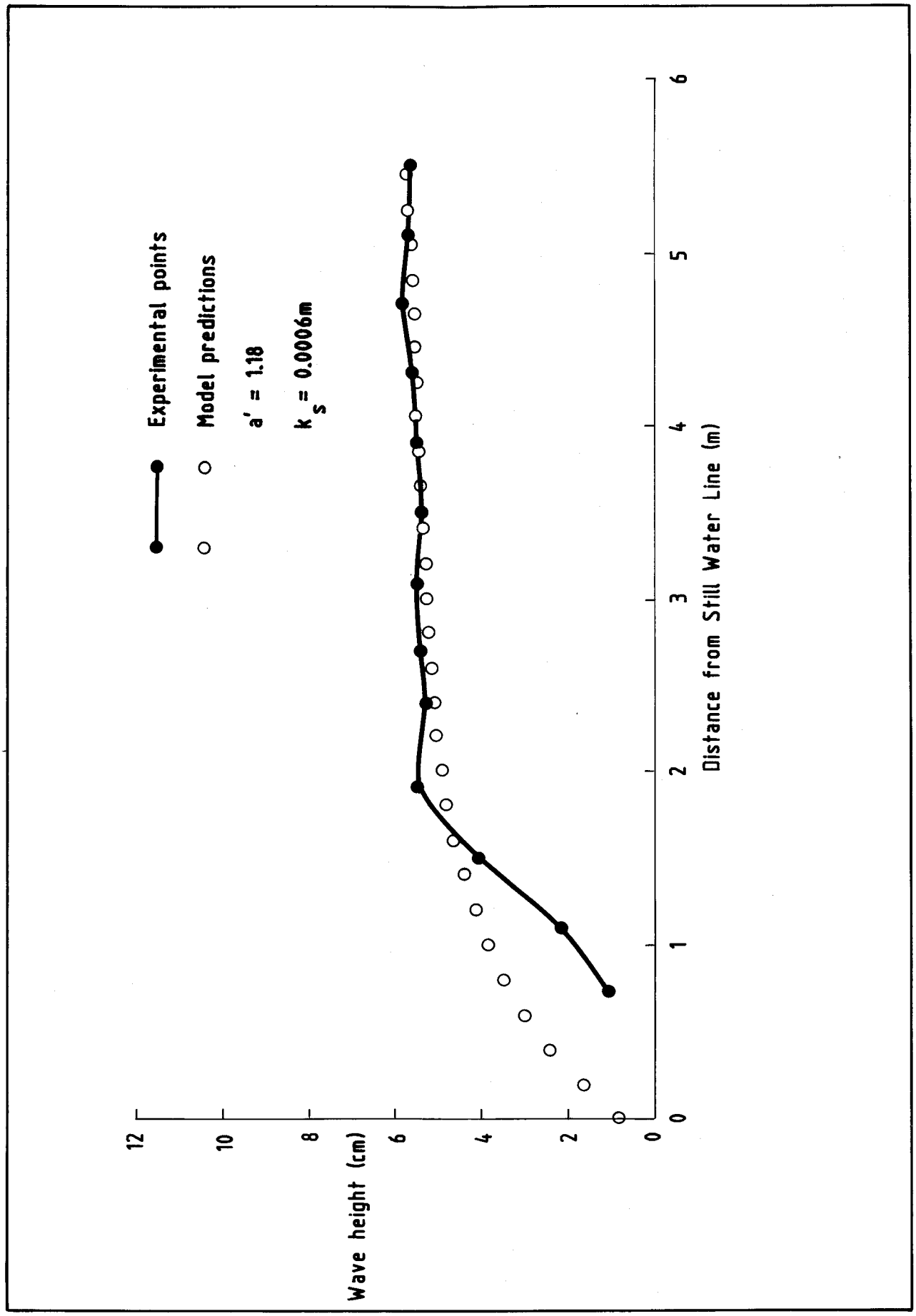

Fig 25 Comparison of Visser Test 6 with Nearshore Profile Model. Wave heights

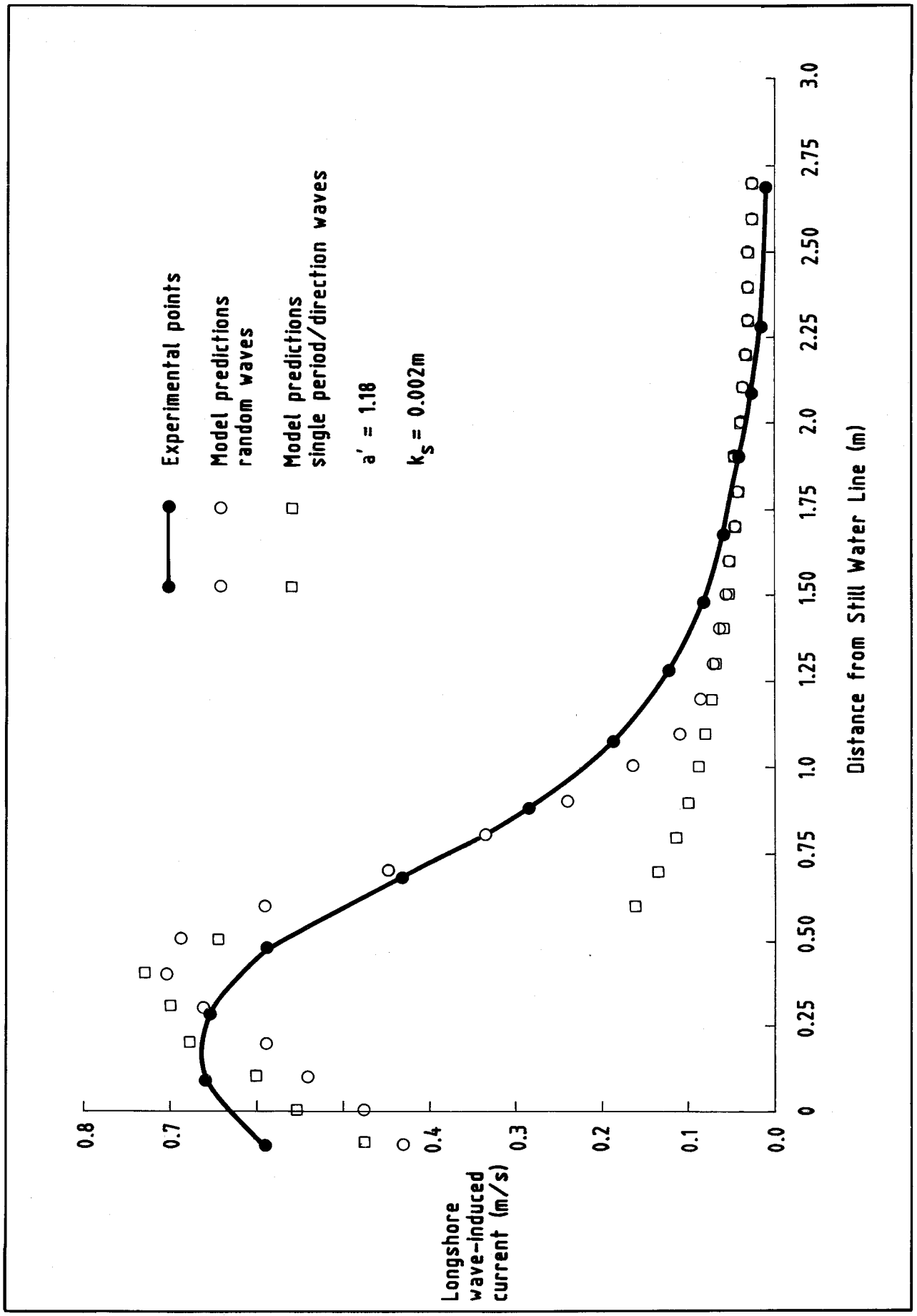

Fig 26 Comparison of Visser Test 1 with Nearshore Profile Model for Random and Single Period/Direction waves. Longshore currents, a' = 1.18

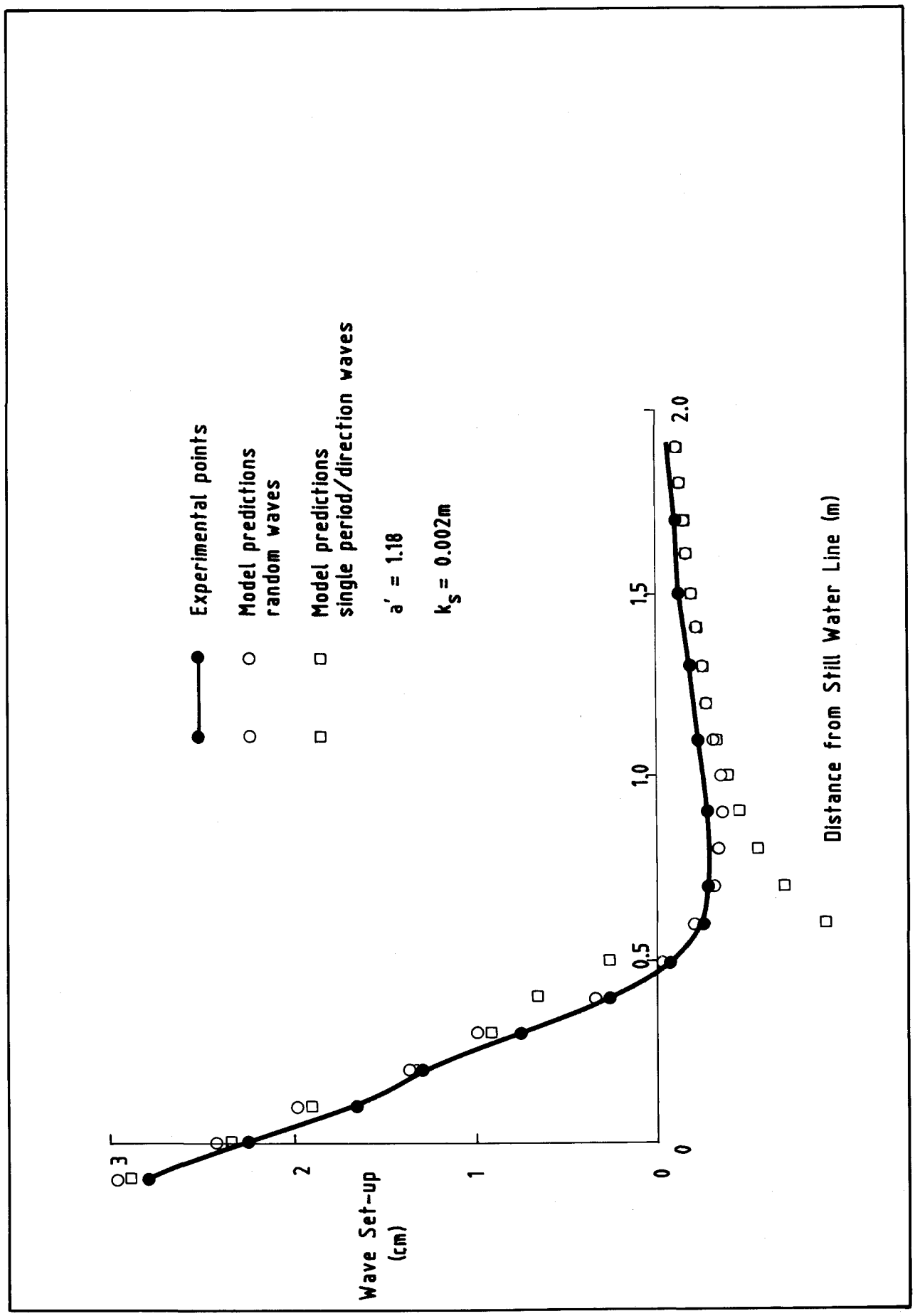

Fig 27 Comparison of Visser Test 1 with Nearshore Profile Model for Random and Single Period/Direction waves. Wave Set-up. a' = 1.18

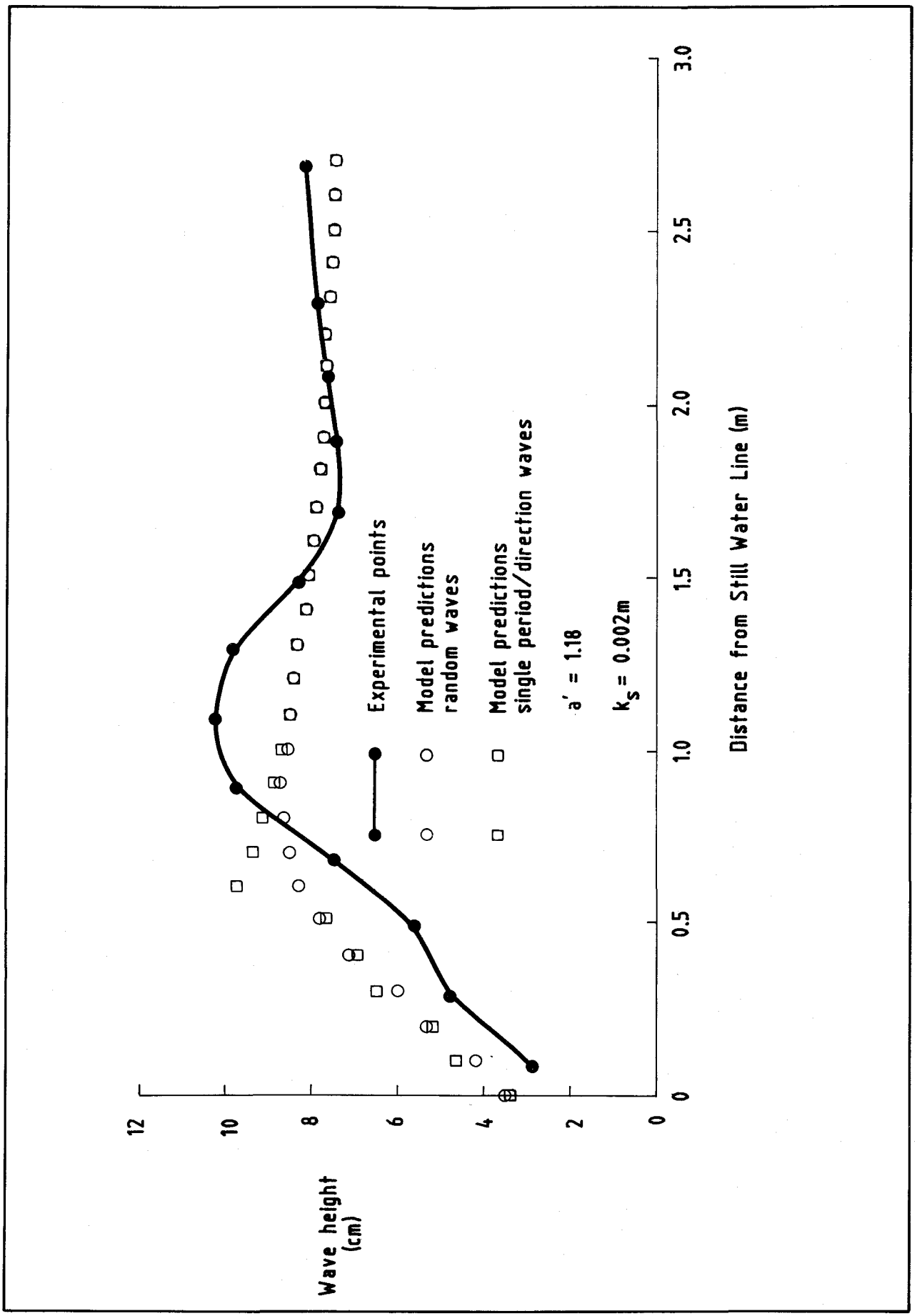

Fig 28 Comparison of Visser Test 1 with Nearshore Profile Model for Random and Single Period/Direction waves. Wave heights. a' = 1.18.

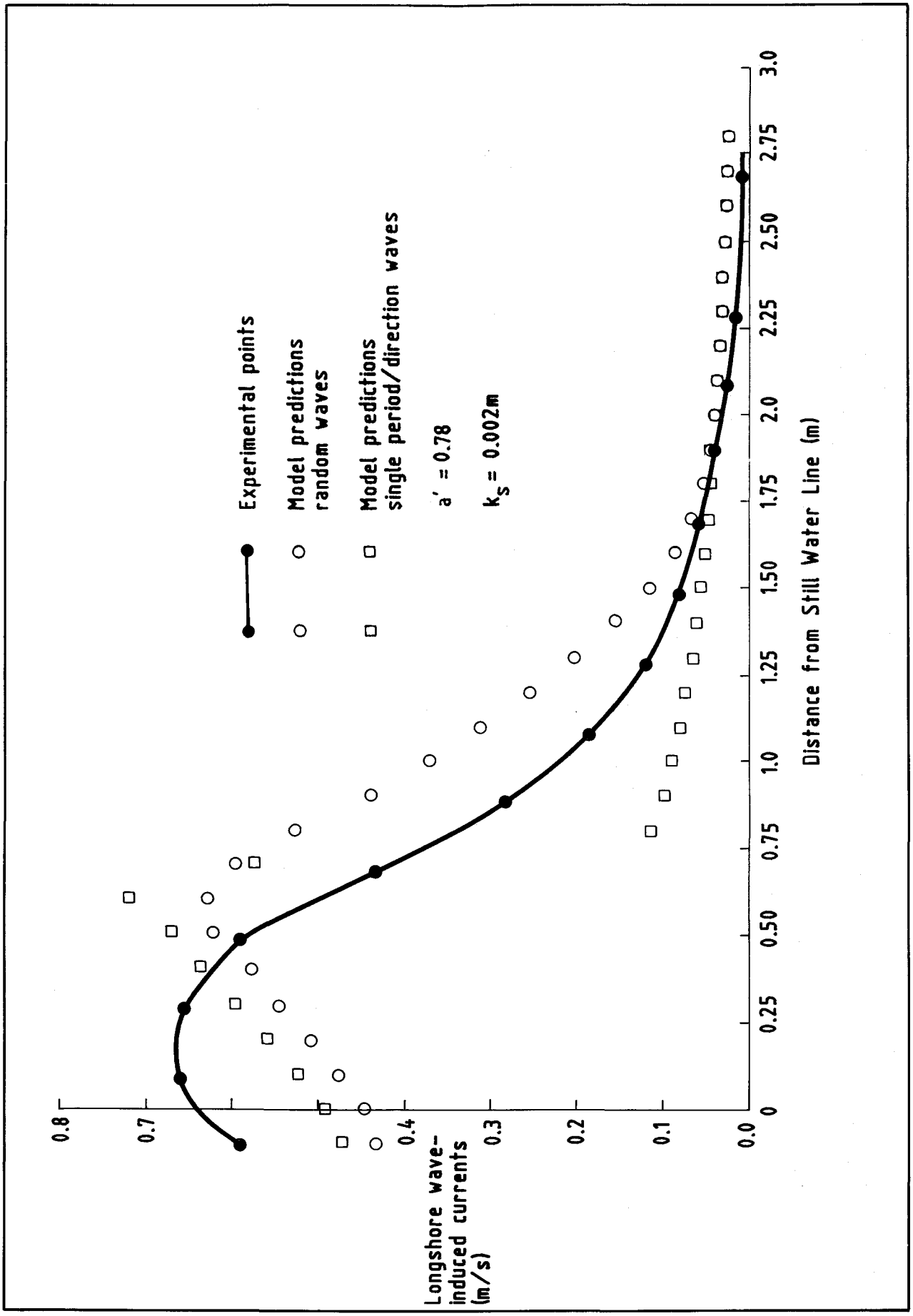

Fig 29 Comparison of Visser Test 1 with Nearshore Profile Model for Random and Single Period/Direction waves. Longshore currents, a' = 0.78

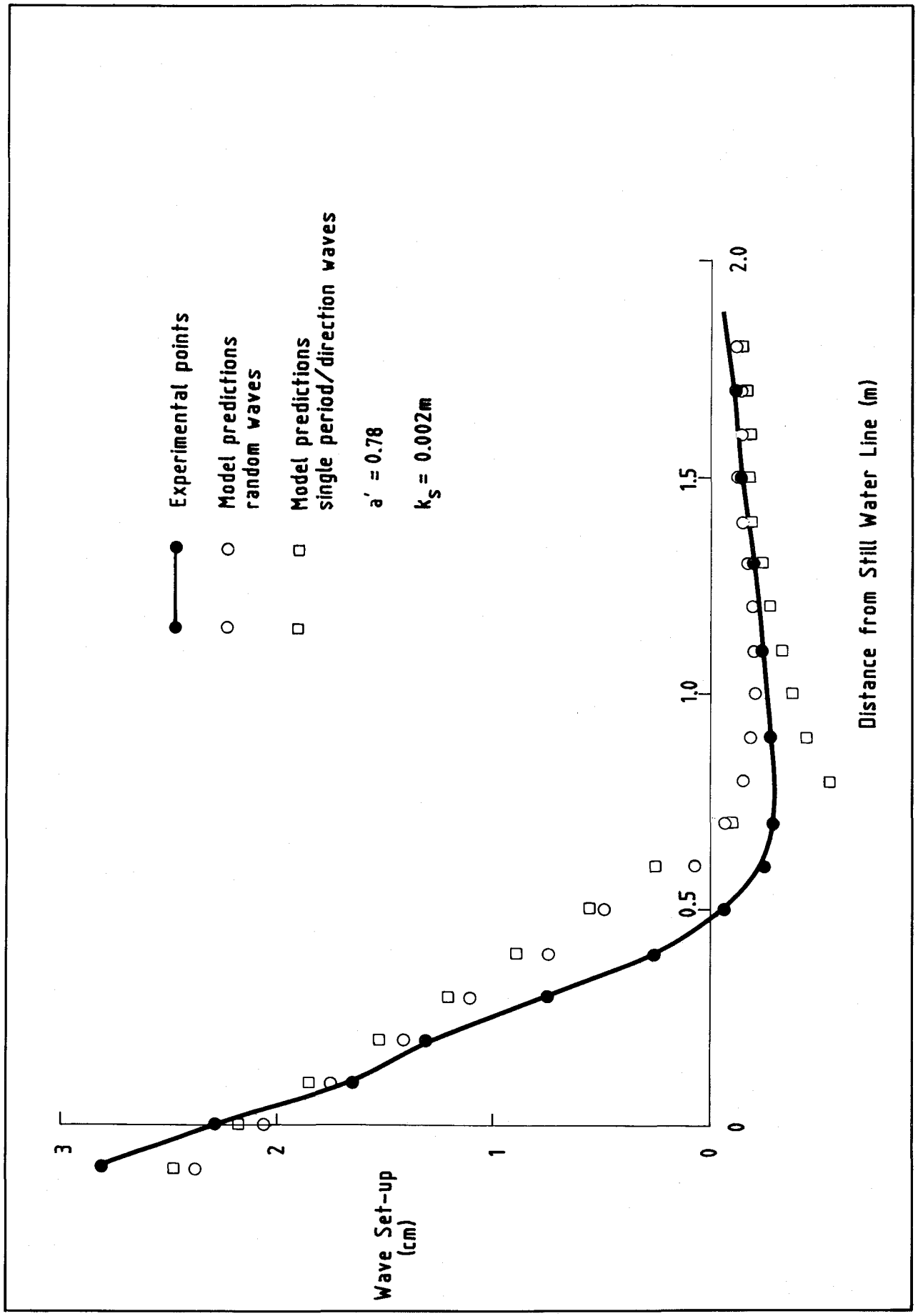

Fig 30 Comparison of Visser Test 1 with Nearshore Profile Model for Random and Single Period/Direction waves. Wave Set-up, a' = 0.78

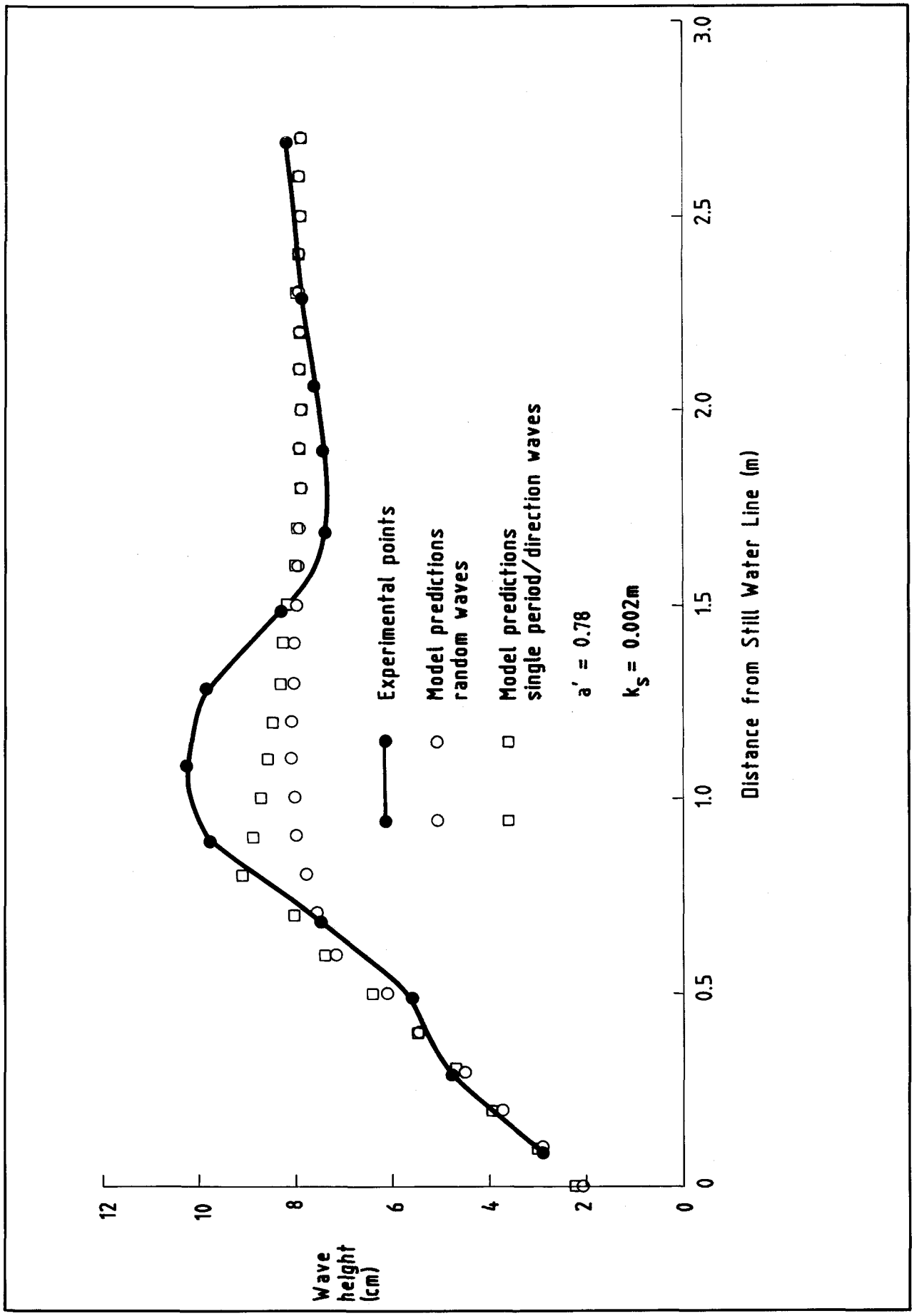

Fig 31 Comparison of Visser Test 1 with Nearshore Profile Model for Random and Single Period/Direction waves. Wave heights. a' = 0.78

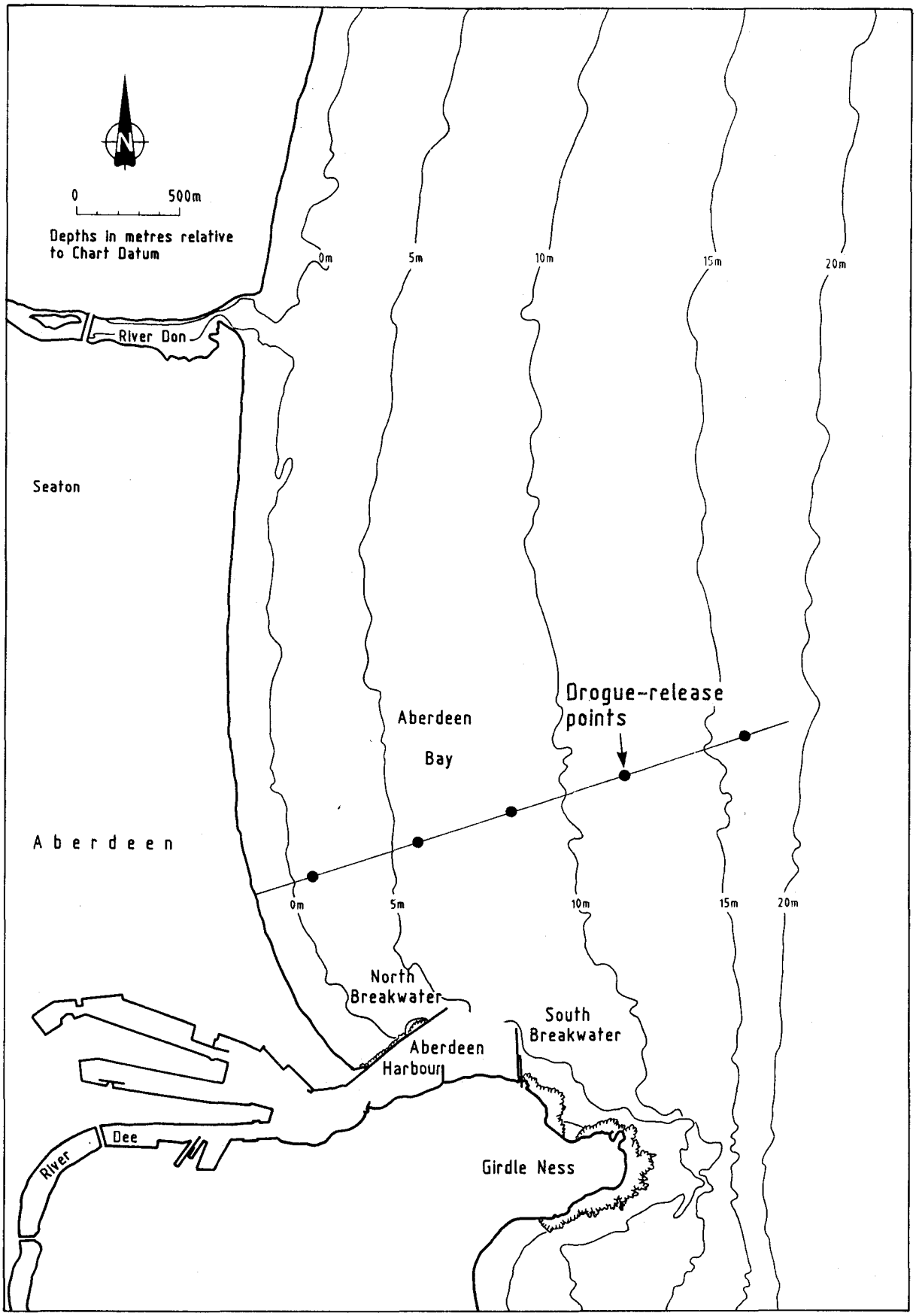

Fig 32 Location of Aberdeen Harbour showing Drogue-release points

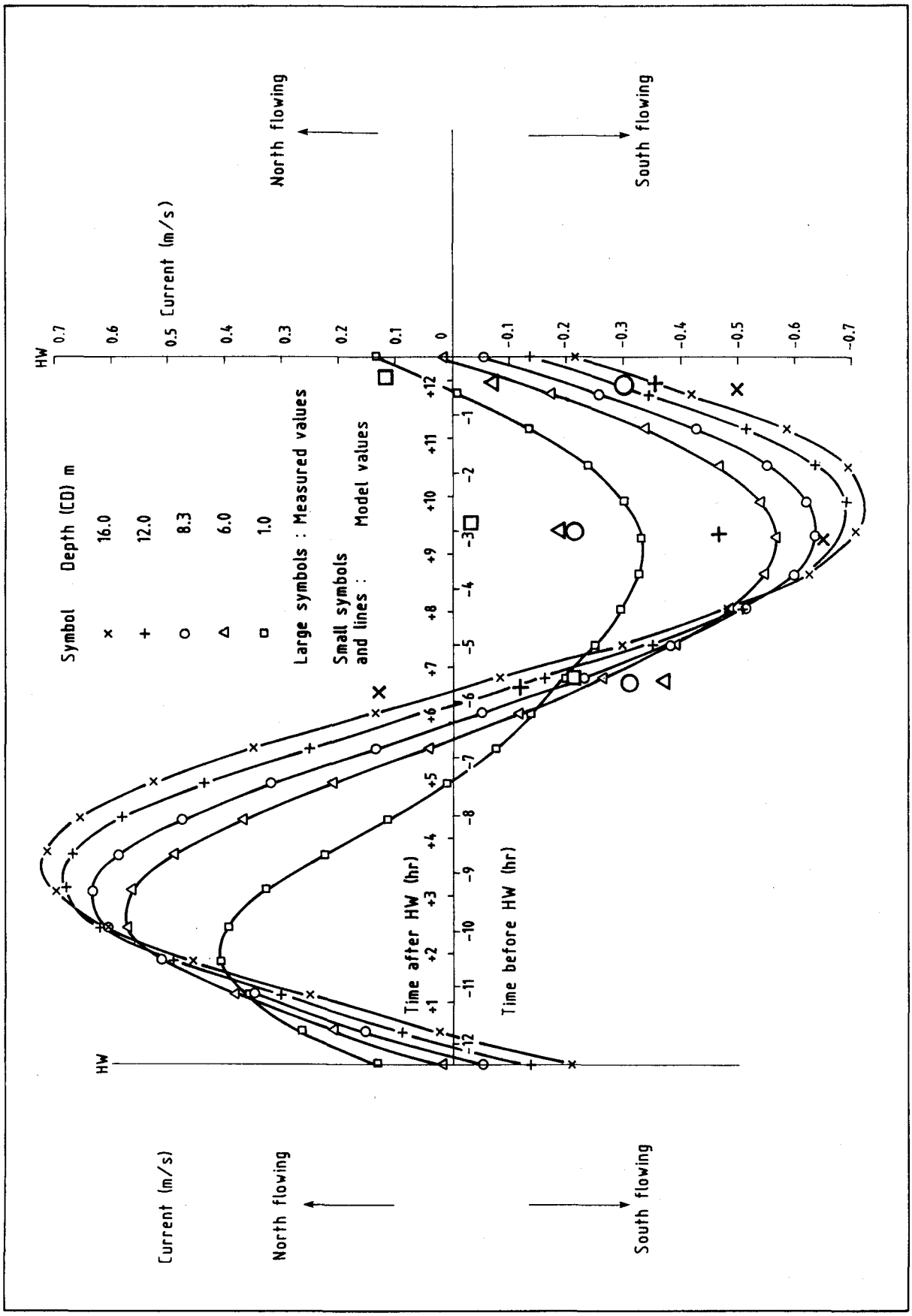

Fig 33 Comparison of tidal current velocity measurements at Aberdeen with predictions from the Nearshore Profile Model